IS-T-788

ELECTRONIC TRANSITIONS OF SOME PI-MOLECULAR CHARGE TRANSFER COMPLEXES

Robert Lee Beckman

M.S. Thesis Submitted to Iowa State University

Ames Laboratory, DOE
Iowa State University
Ames, Iowa 50011

Date Transmitted: December 1977

PREPARED FOR THE U.S. DEPARTMENT OF ENERGY
UNDER CONTRACT NO. W-7405-eng-82

DISCLAIMER

NOTICE

Available from: National Technical Information Service
U. S. Department of Commerce
P.O. Box 1553
Springfield, VA 22161

Price: Microfiche $3.00

Electronic transitions of some pi-molecular charge transfer complexes

by

Robert Lee Beckman

A Thesis Submitted to the
Graduate Faculty in Partial Fulfillment of
The Requirements for the Degree of
MASTER OF SCIENCE

Department: Chemistry
Major: Physical Chemistry

Approved:

Gerald J. Small
In Charge of Major Work

Robert J. Angelici
For the Major Department

For the Graduate College

Iowa State University
Ames, Iowa

1977

TABLE OF CONTENTS

Electronic transitions of some pi-molecular charge transfer complexes

Robert Lee Beckman

Under the supervision of Gerald J. Small
From the Department of Chemistry
Iowa State University

Previously, only the optical study of neat crystals of anthracene-pyromellitic dianhydride (A-PMDA) has revealed the sharp zero-phonon and multi-phonon structure necessary for a quantitative description of the exciton-phonon (for neat crystal) or electron-phonon (for guests of mixed crystals) coupling in π-molecular charge transfer (CT) complexes.

A unique phonon progression in the phosphorescence spectrum of pyrene-PMDA (Py-PMDA) in naphthalene-PMDA (N-PMDA) is reported here. Calculations of the electron-phonon coupling strength parameter for the ground and excited states indicate strong coupling for the fractional CT contribution of Py-PMDA to the observed phosphorescent state. Model calculations indicate that the observed low frequency phonon mode corresponds to a low energy rotation of the

---

Work performed for the U.S. Energy Research and Development Administration under Contract No. W-7405-eng-82.

rigid guest complex and not a symmetric donor-acceptor stretch. The unusual reduction of the phonon mode frequency in the excited as compared to that of the ground state is explained in terms of a contracted complex that can more easily rotate in a larger cavity.

A brief phonon progression is also observed for the mixed crystal A-PMDA in N-PMDA.

For both mixed crystals, Py-PMDA in N-PMDA and A-PMDA in N-PMDA, the energy spacing between the zero-phonon vibrational bands in the mixed CT crystal phosphorescence spectrum are very similar to those obtained from the phosphorescence spectrum of the pure donor in a rigid matrix. There is a large blue shift between the origin band of the mixed CT crystal phosphorescence spectrum and the origin band of the pure donor phosphorescence spectrum for the A-PMDA mixed crystal, but not for the Py-PMDA mixed crystal.

The structureless CT absorption spectra of Py-PMDA and A-PMDA mixed crystals indicate strong electron-phonon coupling, as does the structureless CT fluorescence spectrum of A-PMDA in N-PMDA. We do not observe any CT fluorescence that can be conclusively attributed to Py-PMDA.

The CT absorption and emission spectra of the neat N-PMDA host reveal no sharp structure, indicating strong-exciton-phonon coupling. The particularly long absorption tail observed for N-PMDA neat crystals supports the contention that N-PMDA may be disordered.

INTRODUCTION

For the past several years, a great deal of attention has been given to systems where the transfer of an electron from a donor molecule to an acceptor molecule has resulted in pseudo-one-dimensional behavior. This thesis studies one class of a growing number of systems that one collectively called charge transfer (CT) complexes. The study will focus on the optical spectra of mixed crystals of anthracene-pyromellitic dianhydride (A-PMDA) and pyrene-PMDA (Py-PMDA) guests in a naphthalene-PMDA (N-PMDA) CT host.

Classification of CT Complexes

The CT systems studied here and discussed below have been restricted by binary complexes of π-molecular donors and acceptors. Binary mixtures of organic compounds can be divided into two major groups (1). The groups are distinguished by classifying the lowest lying singlet excitation. If this lowest excited state is a singlet state of one of the two components of the mixture, the compound is classified as a π-molecular crystal. The second group is composed of π-molecular charge transfer complexes, each of which has a new state, called a charge transfer state, which is lower in energy than either of the lowest singlets of the two components.

The class of CT complexes can be further categorized. The first subclass is composed of radical ion salts characterized by their ionic ground states and high electrical conductivity. The second subclass is composed of complexes that are insulating in their ground states. This latter type of complex will be considered here.

Geometric Characteristics

Both classes of CT complexes have similar distinguishing physical characteristics. One of these characteristics is the face-to-face stacking of the aromatic rings of the molecule. There are two variations of this geometry. One has segregated stacks of donors and acceptors with TTF-TCNQ being an example. The other geometry, which is typical of the complexes studied here, has stacks of alternating donor/acceptor molecules. It is impossible to predict which of the two types of geometry a complex will form using existing theories.

Along the stacks the ground electronic state interplanar distances are approximately 3.1 to 3.5 Å, which is less than the 3.5 to 3.6 Å distances expected for Van der Waals repulsion for π-electron systems. This close packing is indicative of the enhanced orbital overlap that occurs along the stack. For the alternating donor/acceptor geometry, the overlap lies along the axis of the transfer of an electron from the donor to the acceptor.

Interactions between stacks are typical of those expected for nonoverlapping molecular solids. Thus, it is not surprising that the crystals exhibit pseudo-one-dimensional characteristics.

Charge Transfer State

The formation of the new low-lying electronic CT state will result in optical absorption and fluorescence spectra characteristic of the complex with the associated CT states usually lying in the UV or visible region.

The CT complexes possessing a neutral ground state are considered weaker CT complexes than ion salt radicals such as TTF-TCNQ. This is because the neutral ground state complexes are insulating in their ground state with only a partial transfer of an electron occurring. The excited singlet state of the complex will correspond to an almost complete transfer of an electron from the highest filled donor orbital to the lowest unfilled acceptor orbital. The resulting excited state will be highly polar. The transfer of charge can be represented as

$$|\ldots\ DADA\ \ldots\rangle \xrightarrow{h\nu_{CT}} |\ldots\ DA^{-}D^{+}A\ \ldots\rangle \qquad (1)$$

The situation is almost reversed for ion radical salts such as TTF-TCNQ which have polar, conducting ground states and insulating excited states.

In this thesis, the absorption, fluorescence and phosphorescence spectra of mixed crystals of anthracene-pyromelletic dianhydride (A-PMDA) and pyrene-PMDA (Py-PMDA) in naphthalene-PMDA (N-PMDA) will be studied with the focus on understanding the CT electron-phonon interaction which is so instrumental in determining the spectra profiles.

For the case where sharp zero-phonon transitions with accompanying phonon side bands are observed in the CT optical spectra one can hope to extract quantitative information on the electron-phonon interaction. Such sharp structure in the optical spectra of CT complexes is a very rare occurrence as will be illustrated later. We are fortunate to be able to report here the observation of an exceedingly sharp phonon progression in the phosphorescence spectrum of Py-PMDA in a N-PMDA host crystal.

Importantly, the phosphorescence triplet has a high degree of CT character.

LITERATURE REVIEW: PREVIOUS STUDIES

A great deal has been published on the various types of pseudo-one-dimensional charge transfer complexes. A very brief summary emphasizing some of the major review articles and some of the authors who have conducted extensive studies of such systems will be given.

TCNQ Complexes

Perhaps the biggest catalyst to studies of these systems was a report on the extraordinarily high conductivity of tetrathiofulvalinium-tetracyanoquinodimethane (TTF-TCNQ) (2). This study reported on enhancement of the conductivity at 60°K of 500 times the room temperature value. An avalanche of theories and experimental papers both supporting and refuting this report followed. Repeated experimental work, however, has shown the enhancement factor to be more on the order of 100 to 150 (3-5).

Explanations (6,7) have been offered based on the Peierls-Fröhlich transition (8,9) as to why TTF-TCNQ does not display superconductivity. Heegar and Garito (4,5), members of the group that originally reported the anomalous conductivity, later agreed that the charge density wave will cause a three-dimensional ordering transition (i.e., interactions between the chains) in which the phase of the wave is pinned by impurity centers and lattice defects. This causes a

transition to an insulating state before the crystal becomes superconducting.

Other TCNQ salts have been studied as well. Reviews by Heegar and Garito (10) and by Shchegolev (11) list several TCNQ salts and discuss their conductivity.

Tetrahalobenzoquinone Complexes

Many of the investigations of charge transfer complexes involving tetrahalobenzoquinone acceptors such as fluoranil, chloranil, bromanil and iodonil have been restricted to solution studies since the complex is not formed by evaporation of the solvent. We have tried to grow crystals from solution but have only obtained the starting components, which seem to be much more insoluble than the complexes. Melt grown samples gave inhomogeneous solids which decomposed when zone refined.

Structure determinations (12-17) have been made for a few of the complexes that form crystals from solution. Other studies involved the determination of thermodynamic constants from NMR shift measurements (18), and of ionization potentials for aromatic donors (19), reports of absorption spectra of the complexes in solution (20,21) and the solid state (22), as well as some electrical conductivity studies (23).

We felt, however, that such studies did not demonstrate any unusual or unexpected behavior and that problems of

photolysis reactions of acceptors (24), decomposition of crystals due to their volatility and effects due to the choice of solvents used to grow the crystals (25-27) deemed other systems more promising.

TNB Complexes

Another system of complexes that has been studied by this group uses 1,3,5-trinitrobenzene (TNB). Other studies have reported conductivity (28,29), NMR (30) and optical (31,32) spectra and crystallographic information (33,34) for various donor-TNB complexes. However, most of the pertinent work has involved the anthracene-TNB (A-TNB) complex.

The crystal structure (35) of A-TNB has been determined. The unit cell is C2/c with 4 molecules of complex per unit cell. The plane-to-plane stacking is along c. Optical spectra have been published by Tanaka and Yoshihara (36) and Hochstrasser, Lower and Reid (37-39). Similar spectra were recorded by the two groups but each group obtained different polarization ratios. In addition, the latter group reported an irreversible discontinuity of the fluorescence intensity with varying temperature (39). A Davydov splitting of approximately 200 cm^{-1} due to two translationally inequivalent complexes has also been reported (37). A later study by Beckman, Hayes and Small (40) concluded that the temperature effects reported above were due to strain induced into

crystals grown between quartz discs. However, discontinuities in CT fluorescence intensity with temperature, along with supportive Raman evidence, indicate a phase transition may occur in A-TNB at ~80°K.

It should be noted that all the absorption and emission spectra consist of broad peaks of several hundred wavenumbers with no fine structure. No zero phonon transitions or low frequency intra-charge-transfer vibrational or phonon structures are observed in neat crystals, glasses or mixed crystals.

TCNB Complexes

Tetracyanobenzene (TCNB) complexes are some of the more studied π-electron insulating charge transfer systems. The most interesting work done with these systems has involved studies of the triplet state. The phosphorescence and ESR spectra of several complexes have been explained in terms of a locally excited triplet state of the acceptor, a locally excited triplet state of the donor or a charge transfer triplet, depending upon the donor used (41). The absorption bands due to transitions from a charge transfer triplet state to a higher triplet state have also been observed (42). Some of the early fluorescence spectra of several TCNB complexes were explained in terms of structure changes involving the surrounding environment (43,44), but later

interpretations are based upon the formation of a triple complex ($D_2^+A^-$) formed in the excited state (45).

One of the few mixed charge transfer crystal studies involved donor-TCNB guests in a different donor-TCNB host. Phosphorescence and ESR measurements show temperature-dependent exciton diffusion rates. This was attributed to self-trapping of the exciton due to rearrangement of the charge distribution resulting from distortions in the lattice upon excitation (46). Methods for determining the relative charge transfer triplet energies from the trap depths have been proposed (47). This is a temperature region where the ESR signal intensity strongly decreases with increasing temperature. This corresponds to thermal depopulation of the traps and is related to the difference (ΔE) between the guest and host triplet states by the expression (47)

$$I \propto \exp(-\Delta E/kT) \qquad (2)$$

where I is the intensity of the ESR signal, k is Boltzmann's constant and T is the temperature. By measuring the ESR zero-field-splitting parameters D and E, the degree of electron delocalization in the triplet state can be calculated (48). These parameters measure the dipole interaction of the two unpaired electron spins in the triplet state and are sensitive to the changes in electron configurations that occur during complex formation. The partial charge transfer

in the charge transfer triplet state increases the delocalization of the exciton and the parameters are thus reduced in value (47-51). Unfortunately, the electron delocalization could not be probed directly with the methods applied to the above authors. However, through the improved resolution of the hyperfine structure in the triplet ESR spectra, the electron density near each interacting nucleus can be found. This technique has been applied to various mixed charge transfer systems (52-54) and is now being used for acceptors other than TCNB (54).

A-PMDA

The only previously reported system for which a sharp zero phonon transition has been observed is anthracene-pyromellitic dianhydride (A-PMDA). Optical and ESR spectra have been reported by Haarer and Karl (55) which show broad, structureless emission and absorption bands. However, a sharp zero phonon line was later observed in the absorption spectrum of a thin (170 μ) crystal (56). This peak broadens and loses intensity as the temperature is raised from 2°K to 12°K, where the peak is barely discernible. The fluorescence spectrum shows ten visible satellite peaks accompanying the zero phonon transition. Both absorption and emission spectra are accompanied by phonon sidebands.

The application of an external electric field induces a second zero phonon line 10 cm^{-1} above the lowest zero-phonon absorption (57,58). At zero field, one can make an even or odd wavefunction from the two possible states $A^{-}D^{+}A$ and $AD^{+}A^{-}$. The even combination has no dipole oscillator strength, while the odd function carries all of the strength. By applying an electric field, the zero functions become mixed and both transitions are observed. From the splitting, one can calculate the exciton transfer integral and the change in the dipole moment. Information on the band structure can also be derived from the data of this Stark experiment (58). Haarer derives an expression giving the coherent exciton transfer in terms of the probability of the exciton transfer matrix elements M_e, M_h, M_{2e} and M_{2h} as given by equations (9-12) in the Theory section. From the coherent exciton transfer term, the energy can be calculated for various values of the exciton wavevector k, and thus the band structure can be plotted.

THEORY

Clarification of Terms

In this section we will consider the CT excitation process in terms of a single complex itself and then the analogous excitation in a crystal lattice. First, a few terms will be clarified.

When the complex is excited to the CT state, a bound electron-hole pair is created. In the crystal, this leads to the formation of a CT exciton band. There are two limiting definitions of the exciton. If the electron-hole separation is much smaller than the lattice constants, one has a Frenkel exciton. The "tightly bound" electron-hole pair may still propagate through the lattice due to interactions between the excited and ground state complexes. If the electron-hole pair has a separation that is large in comparison to the lattice constants, it is known as the Mott-Wannier exciton. The crystal systems we have studied fall into the Frenkel exciton category.

Crystal phonons are the low frequency quantized vibrations characterized by the intermolecular forces. They are describable in terms of rotations and translations about three (3) mutually orthogonal directions. For a crystal of N unit cells with p molecules per unit cell, there are three translational (acoustic) branches per unit cell or a total

of 3N acoustic modes for the crystal. Since there are 6pN degrees of freedom for the crystal, the rest of the (6p-3)N degrees of freedom are accommodated by the optic modes (6p-3 optic branches). Each branch contains N modes with each mode characterized by an irreducible representation of the translational group of the crystal or a specific value of the reduced wave vector $\bar{q}$.

CT Hamiltonian without Lattice Interactions

The hamiltonian for a 1:1 donor/acceptor charge transfer (CT) crystal may be written as (59)

$$H = H_o + H_{site} + H_m \tag{3}$$

Here H_o is the Hubbard hamiltonian for a one-dimensional array of N sites labeled consecutively. It is given as

$$H_o = T \sum_{n\gamma} (f^+_{n\gamma} f_{n+1,\gamma} + f^+_{n+1,\gamma} f_{n\gamma}) + I \sum_n f^+_{n\gamma} f_{n\gamma} f^+_{n\beta} f_{n\beta} \tag{4}$$

Here,

$$T = \langle D^+A^- | H_{sc} | DA \rangle \tag{5}$$

is the Mulliken CT integral (59-61) (for nearest neighbors) and H_{sc} is the complete hamiltonian for a single complex (sc). The term I is the intrasite coulombic repulsion between two electrons on the same site n (I>0). The

operators $f^{+}_{n\gamma}$, $f_{n\gamma}$ create and annihilate, respectively, an electron with spin γ at the n^{th} site.

The term H_{site} describes the inequivalence of the donor (D) and acceptor (A) sites and is given as

$$H_{site} = \sum_{n\gamma} (-1)^{n} E_{o} f^{+}_{n\gamma} f_{n\gamma} \tag{6}$$

The term E_o can be estimated from

$$2E_{o} - I = I_{D} - A_{A} \tag{7}$$

where I_D is the donor's ionization potential and A_A is the electron affinity of the acceptor.

To provide for only a partial tranference of the electron from the donor to the acceptor, H_m, given as

$$H_{m} = \frac{-MN}{2} \rho_{A}^{2} \tag{8}$$

is added. Here M is the Madelung constant and depends on the full three-dimensional lattice. It represents the coulomb stabilization per $D^{+}A^{-}$ unit cell. N is the number of electrons. The term ρ_A is the ground-state charge density on the A sites and is a measure of the ionicity.

Transition Matrix Elements

The simple theory above is not practical for explaining lattice-exciton interactions or any other dynamic processes.

However, before such a theory is developed, we will consider the types of interactions that can occur between different sites in the stack. Specifically, the transfer or movement of the CT excitation within the crystal will be considered. The most probable transitions are shown schematically in Figure 1. The matrix elements describing these transitions constrained to interactions between nearest donors, nearest acceptors and the nearest donor and acceptor can be given as (58)

$$M_1 = \langle\psi(j,\alpha)|H|\psi(j+1,\sigma)\rangle$$
$$= \langle\psi(j+1,\sigma)|H|\psi(j,\sigma)\rangle, \tag{9}$$

$$M_h = \langle\psi(j,+\tfrac{1}{2})|H|\psi(j+1,-\tfrac{1}{2})\rangle \tag{10}$$

$$M_e = \langle\psi(j,+\tfrac{1}{2})|H|\psi(j,-\tfrac{1}{2})\rangle \tag{11}$$

$$M_{2h} = \langle\psi(j,+\tfrac{1}{2})|H|\psi(j+2,-\tfrac{1}{2})\rangle \tag{12}$$

and

$$M_{2e} = \langle\psi(j,+\tfrac{1}{2})|H|\psi(j-1,-\tfrac{1}{2})\rangle \tag{13}$$

where the electrons are promoted from any donor molecule $j=1,2,\ldots N$ to the nearest acceptor molecule on the right ($\sigma=+\frac{1}{2}$) or the left ($\sigma=-\frac{1}{2}$). The localized charge transfer states are denoted by $\psi(j,\sigma)$.

THIS PAGE

WAS INTENTIONALLY

LEFT BLANK

Figure 1. Schematic representation of the most probable CT exciton (electron) transfer process. (a) Transfer to a neighboring complex, (b) a hole transfer, (c) an electron transfer, (d) sum of (a) and (b), (e) sum of (a) and (c). Note that process (a) is the only process that occurs without polarity flipping

$$\cdots A\ D^{+}A^{-}D\ A\ \cdots$$
$$\cdots A\ D\ A\ D^{+}A^{-}\ \cdots$$

(a) M_1

$$\cdots A\ D^{+}A^{-}D\ A\ \cdots$$
$$\cdots A\ D\ A^{-}D^{+}A\ \cdots$$

(b) M_h

$$\cdots D\ A^{-}D^{+}A\ D\ \cdots$$
$$\cdots D\ A\ D^{+}A^{-}D\ \cdots$$

(c) M_e

$$\cdots D^{+}A^{-}D\ A\ D\ A\cdots$$
$$\cdots D\ A\ D\ A^{-}D^{+}A\cdots$$

(d) M_{2h}

$$\cdots D\ A^{-}D^{+}A\ D\ A\ \cdots$$
$$\cdots D\ A\ D\ A\ D^{+}A^{-}\cdots$$

(e) M_{2e}

Note that M_1 is independent of the direction of electron transfer σ. This matrix element describes the transfer of an excitation from one DA pair to its neighbor complex. Longer range transfers of this type are not considered. This is the only process where polarity flipping (in which the transition dipole is rotated 180°) does not occur. In all of the other processes, polarity flipping does occur. M_e describes the transfer of an electron with the hole remaining stationary. The term M_h describes the hole transition with the electron remaining stationary. The processes M_{2e} and M_{2h} are sums of (M_1+M_e) and (M_1+M_h), respectively. M_1 is a CT excitation propagation between translationally equivalent sites where as the other terms involve translationally inequivalent sites.

Hamiltonian for Exciton-Phonon Coupling

We will now consider the hamiltonians that describe the interactions between the excitons and crystal vibrations (phonons). Because only approximate solutions can be obtained, the final outcome will be dependent on whether one starts with a localized or delocalized exciton description.

The hamiltonian for coupling between a localized exciton and delocalized phonons has been given as (62)

$$H = H_{ex} + H_{ph} + H^1_{ex-ph} + H^2_{ex-ph} \qquad (14)$$

Here, $H_{ex} = \sum_n [(E + \sum_m' D_{nm}) B_n^+ B_n + \sum_m' M_{nm} B_n^+ B_m]$, (15)

$$H_{ph} = \sum_{q,s} b_{qs}^+ b_{qs} \hbar\omega_s(\underset{\sim}{q}), \tag{16}$$

$$H_{ex-ph}^1 = \sum_{s\underset{\sim}{q}} \sum_{n,m}' [B_n^+ B_m e^{i\underset{\sim}{q}\cdot\underset{\sim}{n}} \underset{\sim}{F}_{nm}(\underset{\sim}{q},s) + B_n^+ B_n e^{i\underset{\sim}{q}\cdot\underset{\sim}{n}} \underset{\sim}{X}_s(\underset{\sim}{q})] \varphi_{\underset{\sim}{q}s} \tag{17}$$

$$H_{ex-ph}^2 = \sum_{s\underset{\sim}{q}} \sum_{nm}' [B_n^+ B_m F_{nm}(\underset{\sim}{q},s) + B_n^+ B_n X_s(\underset{\sim}{q})] \varphi_{\underset{\sim}{q}s} \tag{18}$$

and

$$\varphi_{\underset{\sim}{q}s} = b_{\underset{\sim}{q}s} + b_{-\underset{\sim}{q}s}^+ \tag{19}$$

The operators B^+ and B are the creation and annihilation operators, respectively, of a molecular exciton confined to a site labeled by n or m. The phonon creation and annihilation operators b^+ and b are labeled by the q mode of the s branch.

The hamiltonian for a delocalized exciton coupling with a delocalized phonon has been derived by M. Clarke, et al. (62) by using the transformation

$$B_n^+ = N^{-\frac{1}{2}} \sum_{\underset{\sim}{k}} B_k^+ \exp(-i\ \underset{\sim}{k}\cdot\underset{\sim}{n}) \tag{20}$$

This gives

$$H_{ex} = \sum_{\underset{\sim}{k}} E(\underset{\sim}{k})\ B_{\underset{\sim}{k}}^+\ B_{\underset{\sim}{k}} \tag{21}$$

$$H^1_{ex\text{-}ph} = N^{-\frac{1}{2}} \sum_{s\underset{\sim}{k}q} B^+_{\underset{\sim}{k}+\underset{\sim}{q}} B_{\underset{\sim}{k}} \{F_s(\underset{\sim}{k},\underset{\sim}{q}) + X_s(\underset{\sim}{q})\} \varphi_{\underset{\sim}{q}s} \tag{22}$$

and

$$H^2_{ex\text{-}ph} = N^{-\frac{1}{2}} \sum_{s,\underset{\sim}{k},q} B^+_{\underset{\sim}{k}} B_{\underset{\sim}{k}} \{F_s(\underset{\sim}{k},\bar{\underset{\sim}{q}}) + X_s(\bar{\underset{\sim}{q}})\} \varphi_{\bar{\underset{\sim}{q}}s} \tag{23}$$

where $\underset{\sim}{k}$ is the wave vector of the delocalized exciton and $\underset{\sim}{q}$ is the wave vector of a phonon.

We will define the terms in H_{ex} and H_{ph} in both the localized and delocalized representations first. D_{nm}, appearing in eq. (15), gives the change in dispersion in the Van der Waals interactions between sites n and m upon CT excitation. The term $\sum_m{}' D_{nm} B^+_n B_n$ gives the degree of lattice distortion in the region of site n. D_{nm} is defined as (63)

$$D_{nm} = \langle of|V_{nm}|fo\rangle - \langle oo|V_{nm}|oo\rangle$$

$$= \int(\phi^f_n)^2 V_{nm}(\phi^o_m)^2 d\tau - \int(\phi^o_n)^2 V_{nm}(\phi^o_m)^2 d\tau \tag{24}$$

where V_{nm} is the potential between sites n and m, f labels the excited state for site n and o labels the ground state for site n or m. Note that D_{nm} is independent of the exciton wave vector k.

The term M_{nm} is the resonance interaction term which tends to delocalize the excitation over the various sites. It is defined as (63)

$$M_{nm} = \langle of | V_{nm} | of \rangle$$

$$= \int \phi^{o}_{n}{}^{*} \, \phi^{f}_{m}{}^{*} \, V_{nm} \, \phi^{o}_{m} \, \phi^{f}_{n} \, d\tau \qquad (25)$$

The term $E(\underset{\sim}{k})$ appearing in eq. (21) is the exciton energy. If no exciton-phonon coupling exists, the hamiltonian given in eq. (21) is exact and $E(\underset{\sim}{k})$ would be (62)

$$E(\underset{\sim}{k}) = E + \sum_{m} D_{om} + \sum_{m}{}' \, e^{i\underset{\sim}{k}\cdot\underset{\sim}{m}} \, M_{om} \qquad (26)$$

We now want to consider the terms appearing in $H^{1}_{ex\text{-}ph}$ and $H^{2}_{ex\text{-}ph}$. Again, using the notation of Clarke, et al. (62), the resonance exciton-phonon coupling term $F_{s}(\underset{\sim}{k},\underset{\sim}{q})$ is defined as

$$F_{s}(\underset{\sim}{k},\underset{\sim}{q}) = \sum_{m} e^{i\underset{\sim}{k}\cdot\underset{\sim}{m}} \, F_{om}(\underset{\sim}{q}s) \qquad (27)$$

$$= \sum_{jm} \left[\frac{\hbar}{2I_{j}\omega_{s}(\underset{\sim}{q})}\right]^{\frac{1}{2}} e^{j}_{s}(\underset{\sim}{q}) \{\frac{\partial}{\partial R^{j}_{o}} + e^{iq\cdot m} \, \frac{\partial}{\partial R^{j}_{m}}\} \, e^{i\underset{\sim}{k}\cdot\underset{\sim}{m}} \, M_{om} \qquad (28)$$

where $e^{j}_{s}(\underset{\sim}{q})$ is the j^{th} component of a unit vector along the displacements R^{j}_{m} and I^{j} is the mass coefficient of the mode. Translational displacements are described by j=1,2,3 and rotational displacements by j=4,5,6. The subscripts label the q^{th} mode of the s^{th} branch.

The resonance coupling term describes the "hopping" of the exciton from site to site in the localized representation and the scattering of the exciton in the delocalized

representation. The momentum of the exciton is not necessarily conserved. It may hop or scatter elastically so that its wave vector $\underset{\sim}{k}$ does not change or create a phonon of wave vector $\underset{\sim}{q}$. If a phonon is created, the new wave vector of the exciton would be $\underset{\sim}{k}' = \underset{\sim}{k} + \underset{\sim}{q}$. Thus, as pointed out by Davydov (63), "The number of excitons remains constant while the number of phonons is changed".

The other factor contributing to H^1_{ex-ph} and H^2_{ex-ph} is the dispersion coupling term $X_s(\underset{\sim}{q})$ which, despite its name, does not depend on the wave vector of the exciton or the phonon. It is defined as

$$X_s(q) = \sum_{jm} \left[\frac{\hbar}{2I_j\omega_s(q)}\right]^{\frac{1}{2}} e^j_s(\underset{\sim}{q}) \left\{\frac{\partial}{\partial R^j_o} + e^{i\underset{\sim}{q}\cdot\underset{\sim}{m}} \frac{\partial}{\partial R^j_m}\right\} D_{om} \quad (29)$$

Large values of the term containing $X_s(q)$ in H^1_{ex-ph} and H^2_{ex-ph} indicate large distortions of the lattice upon excitation, i.e., the excited molecule is no longer at its ground state equilibrium position.

Davydov (63) points out that if the resonance coupling (F) contribution is much larger than the dispersion coupling (X_s) contribution, one has weak exciton-phonon coupling. If the reverse situation is true, one has strong exciton-phonon coupling. This means, then, that if large distortions occur upon excitation, one should expect strong exciton-phonon coupling.

In viewing H^1_{ex-ph} and H^2_{ex-ph} in the delocalized basis, eqs. (22) and (23), one associates H^1_{ex-ph} with exciton-phonon scattering processes which destroy the k- sense of the initially prepared k state. H^2_{ex-ph} should be associated with lattice distortions following the CT excitation. As long as $H^2_{ex-ph} << H^1_{ex-ph}$, the concept of delocalized band states characterized by specific values of k has validity. Reversing the inequality means that one should revert to the "localized" form of the hamiltonian since now the excited states of the system are more aptly described as wave packets formed from the plane-wave band states.

Effects of Exciton-Phonon Coupling on Optical Spectra

The absorption and emission band profiles can provide important information on the exciton-phonon interaction. The exact band profiles for real systems cannot be calculated from the hamiltonians given above because the dispersion relationships of the excitons and phonons in any arbitrary are generally not known. However, some general conclusions about band profiles can be inferred from the values of the resonance and dispersion coupling terms. Craig and Dissado (64) report the following trends for optical spectra based on the strength of the exciton-phonon coupling.

If the exciton bandwidth (the energy spread of the exciton levels) is greater than any lattice fundamental but less than any spectrally active intramolecular fundamental, the exciton-phonon coupling depends only on the effects of distortion on the resonance coupling. This is the weak coupling case. The spectra will have origin transitions broadened by the damping effects of the phonons with no lattice vibrational structure.

If only dispersive contributions to the electron-phonon coupling are considered (i.e., we assume the resonance coupling is independent of the lattice distortions) Craig and Dissado (64) predict spectra showing broad phonon envelopes composed of members of a phonon progressions broadened by the dispersive contributions to the hamiltonian.

For weak exciton phonon-coupling, then, where both dispersive and resonance coupling affect the coupling, the spectra should show sharp zero-phonon transitions accompanied by phonon sidebands.

In the strong coupling limit, the dispersion coupling term completely dominates the resonance coupling term which can be neglected. Craig and Dissado's (64) calculations predict broad bands in the spectra devoid of sharp structure.

Experimental Determination of the Electron-Phonon Coupling Strength S

Pryce (65) has determined an expression that will give a numerical factor S that characterizes the electron-phonon coupling strength. Assuming a linear electron-phonon coupling mechanism, the weight P_r of an r-phonon process at T=0 is given as

$$P_r = \frac{S^r}{r!} e^{-S}. \tag{30}$$

If S is approximately 1 or less, the coupling is weak. A value of 10 indicates that the electron-phonon coupling is strong. As indicated earlier, strong coupling tends to broaden phonon progressions into one broad envelope whose shape is that of one formed by folding the 1-phonon band shape over r times.

One can experimentally determine S by evaluating the zero-phonon transition probability. The intensity for the zero-phonon line I_z at T=0 has been given as (66)

$$\frac{I_z}{I_t}(T) \approx \exp\{-S[1 + 6.6(T/\theta_D)^2]\} \tag{31}$$

where I_t is the intensity of the zero-phonon line plus all of the r-phonon lines, and θ_D in the Debye temperature. Harrer has determined θ_D to be $\sim$100°K (56) for A-PMDA and

we will assume a similar temperature for Py-PMDA, thus, the temperature correction above can be neglected and the expression simplifies to (67)

$$\left.\frac{I_z}{I_t}\right|_{T = 2°K} \simeq \exp(-S) \tag{32}$$

Thus, $\frac{I_z}{I_t}$ is just the weight factor P_r given in eq. (41). For the one-phonon transition, then, we will assume

$$\left.\frac{I_1}{I_t}\right|_{T = 2°K} \simeq Se^{-S}, \tag{33}$$

and a ratio of eq. (33) and eq. (32) will give

$$\frac{I_1}{I_z} \simeq S. \tag{34}$$

This model assumes that the force constant is the same for the ground and excited states, i.e., the phonon energy of the ground state is the same as that of the excited state.

EXPERIMENTAL

Purification and Crystal Growth

Pyromellitic dianhydride (PMDA), shown below, naphthalene, anthracene and pyrene were obtained from Aldrich Chemical Company.

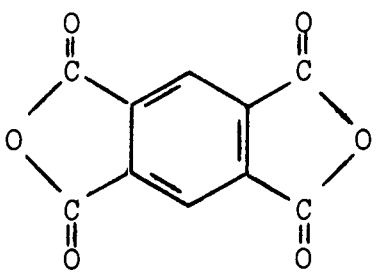

I

PMDA, or 1,2,4,5-tetracarboxylic acid dianhydride

With the exception of pyrene, the remaining compounds were purified by extensive zone refining, undergoing 80 to 150 passes. The pyrene purity was greater than 99% and was used without further purification. The naphthalene was fused with potassium previous to zone refining in order to remove β-methyl naphthalene.

The Py-PMDA and A-PMDA guest complexes were formed by melting the components together in a 1:1 molar ratio under N_2 atmosphere. The complexes were then zone refined, undergoing 80 to 150 passes. Because of N-PMDA's tendency to boil violently when heated, the N-PMDA complex could not be formed and zone refined prior to sample preparation.

Crystals of neat and doped N-PMDA were grown from solution under N_2 atmosphere. The methyl ethyl ketone solvent was redistilled and stored over molecular sieves. Zone refined naphthalene and PMDA were dissolved in a one-to-one molar ratio with the desired molar ratios of zone refined Py-PMDA or A-PMDA complex added.

Sample Mounting

Samples were mounted on a threaded brass plate using black construction paper to retain the crystals. GE low temperature varnish (#7031) was used as the adhesive. Care was taken to insure that the crystals were not actually glued to the paper or the plate, which would cause straining of the crystal upon cooling.

Instrumentation

The spectra were recorded using a Jarrel Ash 1-M model 75-150 Czerny-Turner Fastie spectrometer with grating number 980-43-20-22 blazed for 5000 Å in first order. This instrument has a resolution of 0.10 Å. The dc current detection system used an EMI 9558 QB photomultiplier tube, a Keithley Instrument model 415 picoammeter and an Ortec model 456 H high voltage power supply.

For transmission measurements, a tungsten-iodine source was used. For emission studies, the excitation source was a

Control argon ion laser, model 553U. Stability of this model is not more than 1% drift per hour. For visible excitation lines, a power of approximately 100 mW was used. Laser interference filters (narrow bandpass) were available only for 4579, 4880 and 5145 Å visible lines. For UV excitation, the laser was tuned to give maximum UV output (∿200 mW) and an interference filter was used to separate the 3640 Å line from the 3511 Å line and plasma lines.

Liquid Helium Cryostat

The cryostat used was a metal Janis dewar, model DT, equipped with a tail section containing quartz windows. All spectra, unless otherwise stated, were recorded at approximately 4.2°K. This temperature was achieved by throttling liquid helium to a level just below the sample, allowing the boil-off to cool the sample.

Some of the phosphorescence data of A-PMDA and Py-PMDA were obtained at the λ-point of helium (∿2°K). This temperature is achieved by immersing the sample in liquid helium and pumping on the sample chamber until the λ-point is reached.

RESULTS AND DISCUSSION

Absorption Spectra

The absorption spectra of neat N-PMDA, .015% and .05% A-PMDA in N-PMDA and .015% Py-PMDA in N-PMDA are shown in Figures 2-5. For each spectrum, the upper tracing (solid line) is the actual transmission curve and the lower tracing (dashed wave) is the lamp background. All of the spectra are strongly polarized along the crystal axis that is essentially parallel to the stacking axis.

Disorder in N-PMDA

The primary absorption cut-off for the N-PMDA crystal is shown at the left side of Figure 2 leading to 0% transmission. A band at 22,770 cm^{-1} (750 μ crystal) and 23,060 cm^{-1} (600 μ crystal) is also observed. Since the CT transition is dipole allowed, we do not feel this band is part of the system responsible for the aforementioned primary cut-off. The fact that its frequency is different for the two crystals is not a consequence of the sample thickness but rather that the two crystals come from two different solution-grown batches (both batches were grown under the same conditions). The band also appears in the mixed crystal spectra in Figures 4 and 5. We believe that the long and unusual absorption tail which extends down to $\sim$16,500 cm^{-1} in Figure 2 is a related observation. Recall

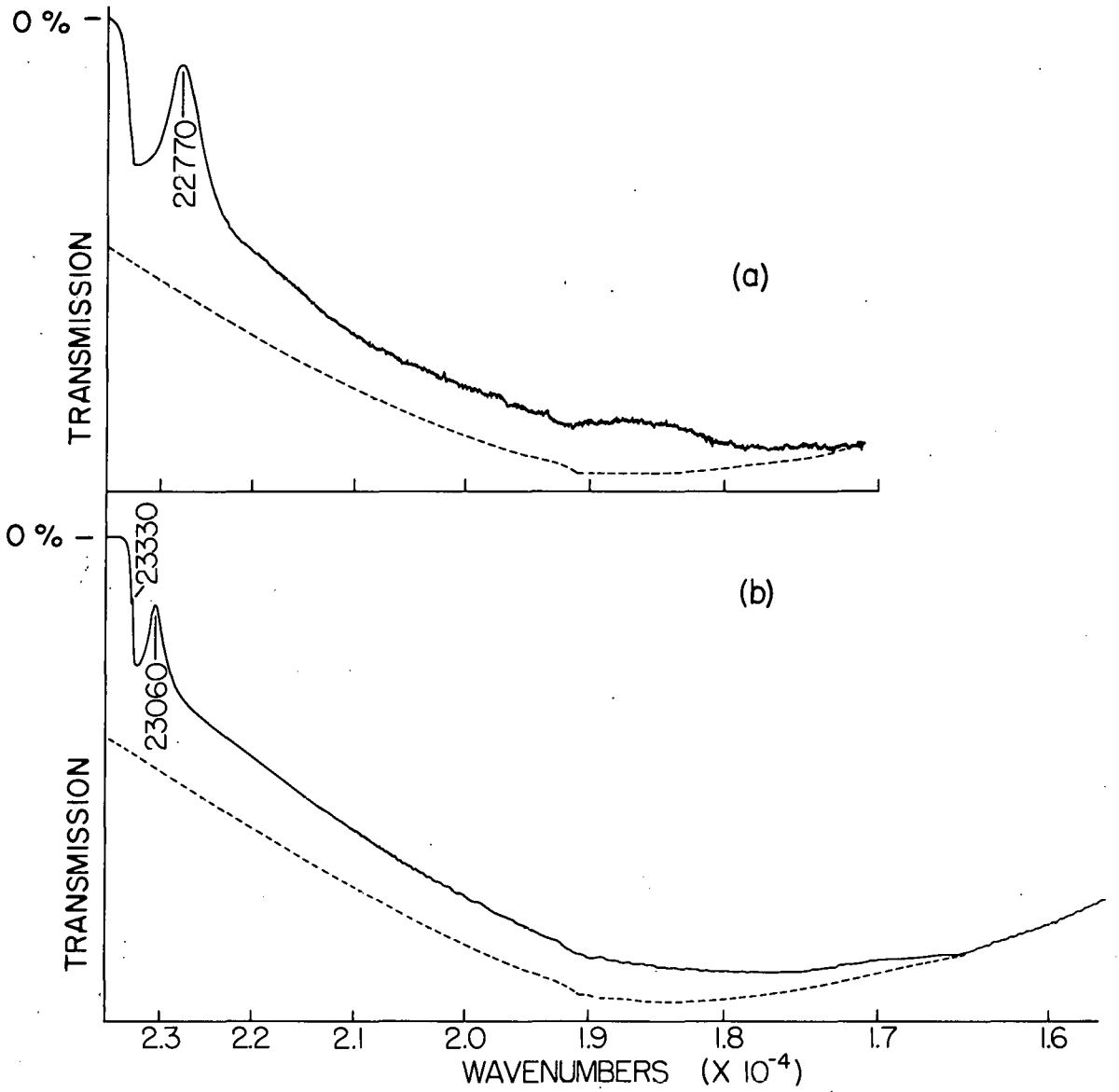

Figure 2. CT absorption spectra of neat crystals of N-PMDA polarized perpendicular to the stacking axis for the two modifications discussed in the test: (a) crystal thickness ∿750 μ, (b) crystal thickness ∿600 μ. The solid line is the actual transmission spectrum, the dashed line is the lamp background. Peak locations are given in units of cm^{-1}.

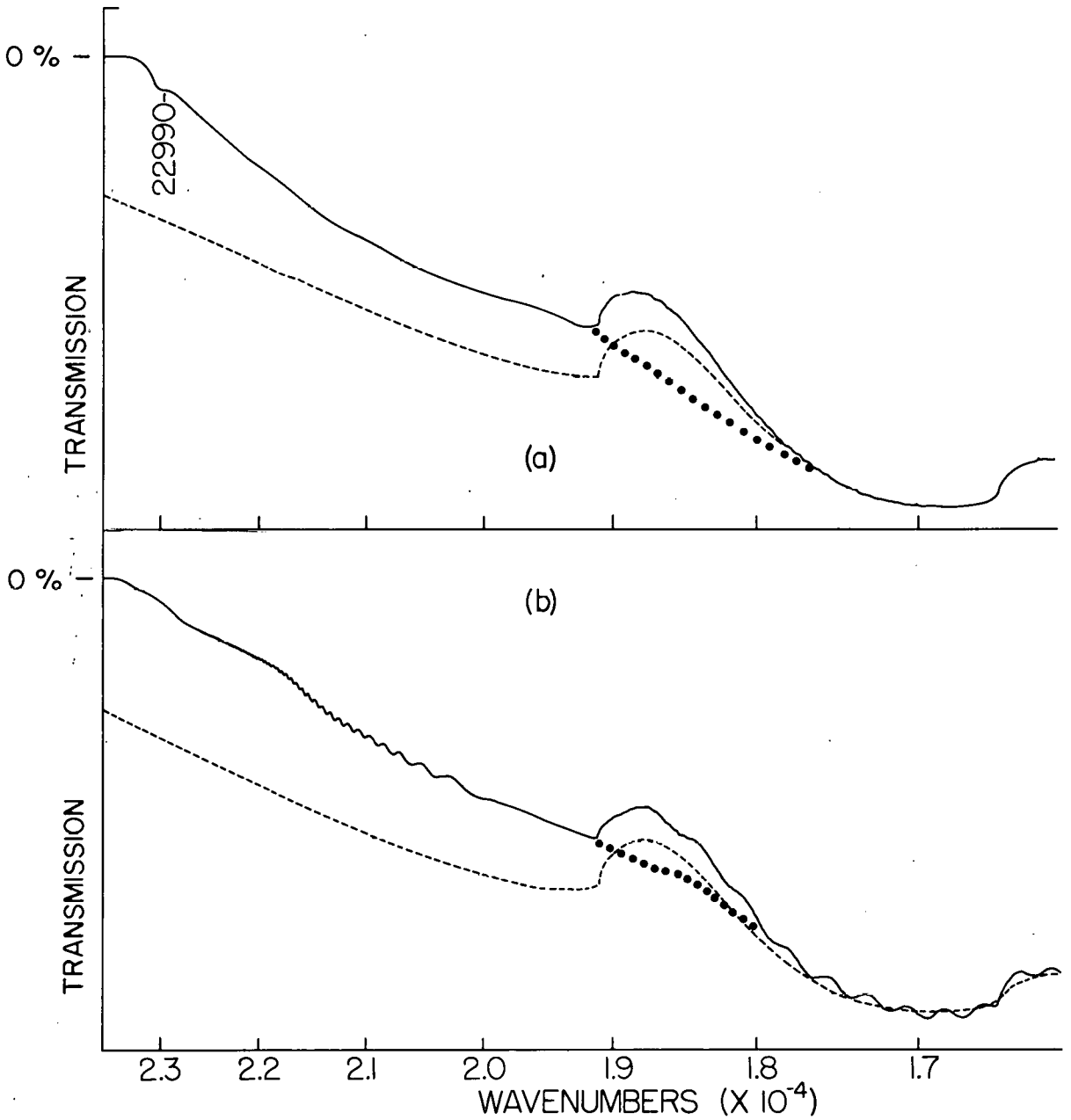

Figure 3. CT absorption spectra polarized parallel to the stacking axis of the complex for (a) the neat N-PMDA crystal shown in Figure 1b, and (b) the .015% Py-PMDA in N-PMDA mixed crystal shown in Figure 4b. Peak location is given in units of cm^{-1}. Refer to Figure 2 for explanation of curves. The dotted line approximates the shape of the transmission curve if the grating effect between 1.9 x 10^{-4} and 1.8 x 10^{-4} wave numbers was removed

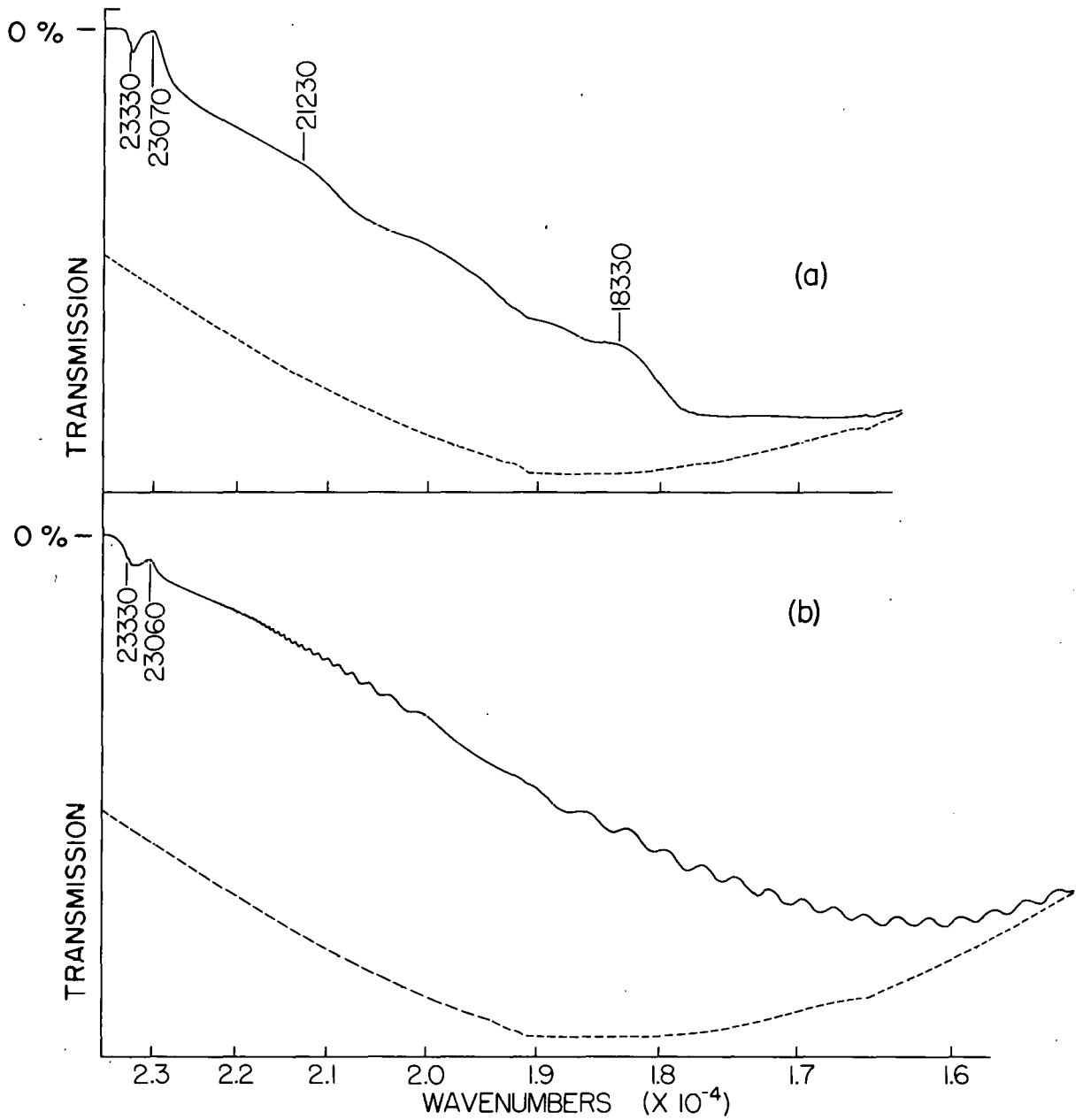

Figure 4. CT absorption spectra of two mixed crystals of .015% Py-PMDA in N-PMDA polarized perpendicular to the stacking axis: (a) ∿850 μ thick crystal, (b) ∿180 μ thick crystal, note the interference patterns. Peak locations are given in units of cm^{-1}. See Figure 2 for explanation of curves.

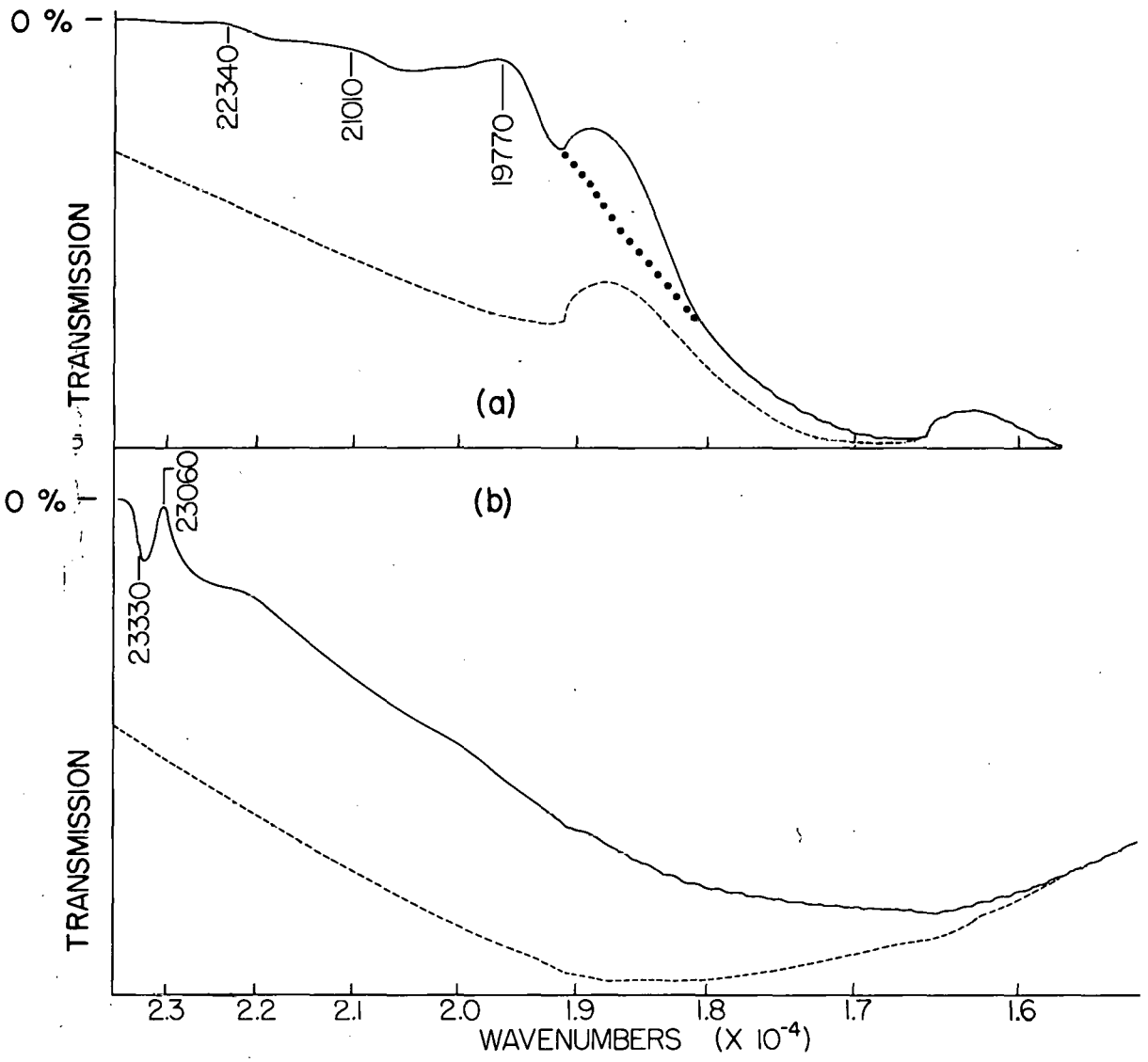

Figure 5. CT absorption spectra of a ∿430 μ thick mixed crystal of .015% A-PMDA in N-PMDA polarized (a) parallel, and (b) perpendicular to the stacking axis. Peak locations are given in units of cm^{-1}. See Figures 2 and 3 for explanation of curves.

that these spectra are recorded at a sample temperature of ca. 4.2°K. Such an absorption tail is difficult to understand unless one proposes that the N-PMDA is disordered. This is the same conclusion reached from X-ray crystallographic studies of N-PMDA down to temperatures as low as 100°K (34). For this reason, we tentatively associate the 23,060 (22,770) cm^{-1} absorption band with crystal disordering and must assume that the exact nature of the disordering is somewhat dependent on crystal growth conditions.

There is another feature appearing in Figure 2b at 23,330 cm^{-1} which is sharp and whose origin is not understood. It does not, however, possess the characteristics of a zero-phonon absorption line associated with the primary absorption cut-off.

The absence, then, of sharp structure (zero-phonon and phonon sidebands) in the absorption spectra and in the emission spectra (discussed later, see Figure 7b) indicates that there is strong exciton-phonon coupling in the N-PMDA crystal. It is essential that high quality crystals be used for this type of study, for crystal defects and strains can rapidly broaden sharp spectral features to the point where they are not observed. In N-PMDA, one has the additional problem of disordering which introduces a distribution of traps into which the CT exciton can scatter. Of course, for strong exciton-phonon coupling, the CT exciton may be self-trapped before such scattering can occur.

Finally, we note that the spectra in Figures 2b and 3a show the transmission interference patterns characteristic of crystal plates of uniform thickness, parallel faces and overall good optical quality.

Mixed crystal absorption spectra

The absorption spectra of Py-PMDA (shown in Figures 3b and 4) and A-PMDA (shown in Figure 5) give broad structureless spectra with no sharp structure. The lowest energy band maxima are 18,330 cm^{-1} for Py-PMDA and 19,770 cm^{-1} for A-PMDA.

The Stokes shift, which is the difference in energy of the lowest band maximum in absorption and the highest band maximum of the emission (see Figure 8), is $\sim$1800 cm^{-1} for A-PMDA. This agrees well with the $\sim$1900 cm^{-1} Stokes shift reported for the neat A-PMDA crystal (55). Such a large Stokes shift is indicative of strong electron-phonon coupling. (In a mixed crystal, the electron-phonon interaction is the analogue to the exciton-phonon coupling of a neat crystal.)

A Stokes shift is not reported here for Py-PMDA because, as we will discuss later, the fluorescence of this complex is questionable.

The zero phonon line is apparently very weak for both the A-PMDA and Py-PMDA guests. It would be, if observed, in

a vicinity midway between the lowest band maximum in absorption and the highest band maximum of the emission.

The lack of sharp structure in the Py-PMDA and A-PMDA CT absorption is another indication of strong electron-phonon coupling in the mixed crystal systems studied.

Emission of A-PMDA in N-PMDA

The emission spectra of two different concentrations (.015% and .05%) of A-PMDA in an N-PMDA host are shown in Figures 6 and 8. The average peak maxima are given in Table 1.

UV excitation of A-PMDA guest and N-PMDA host

A comparison of the 3640 Å (UV) excited CT fluorescence of neat N-PMDA crystals, shown in Figure 7b, with those of the A-PMDA doped crystals given in Figure 6, shows that the peaks located at approximately 22,180 cm^{-1}, 20,960 cm^{-1} and 19,870 cm^{-1} (which is not resolved in the .015% crystal) are emission due to the host. The peaks at 19,200 cm^{-1} in the .05% spectrum and at 19,360 cm^{-1} in the .015% spectrum arise with the introduction of the A-PMDA impurity but remain largely unexplained. It is possible that disorder due to the presence of the guest or a macromolecule formed by guest/host interactions is responsible for these peaks.

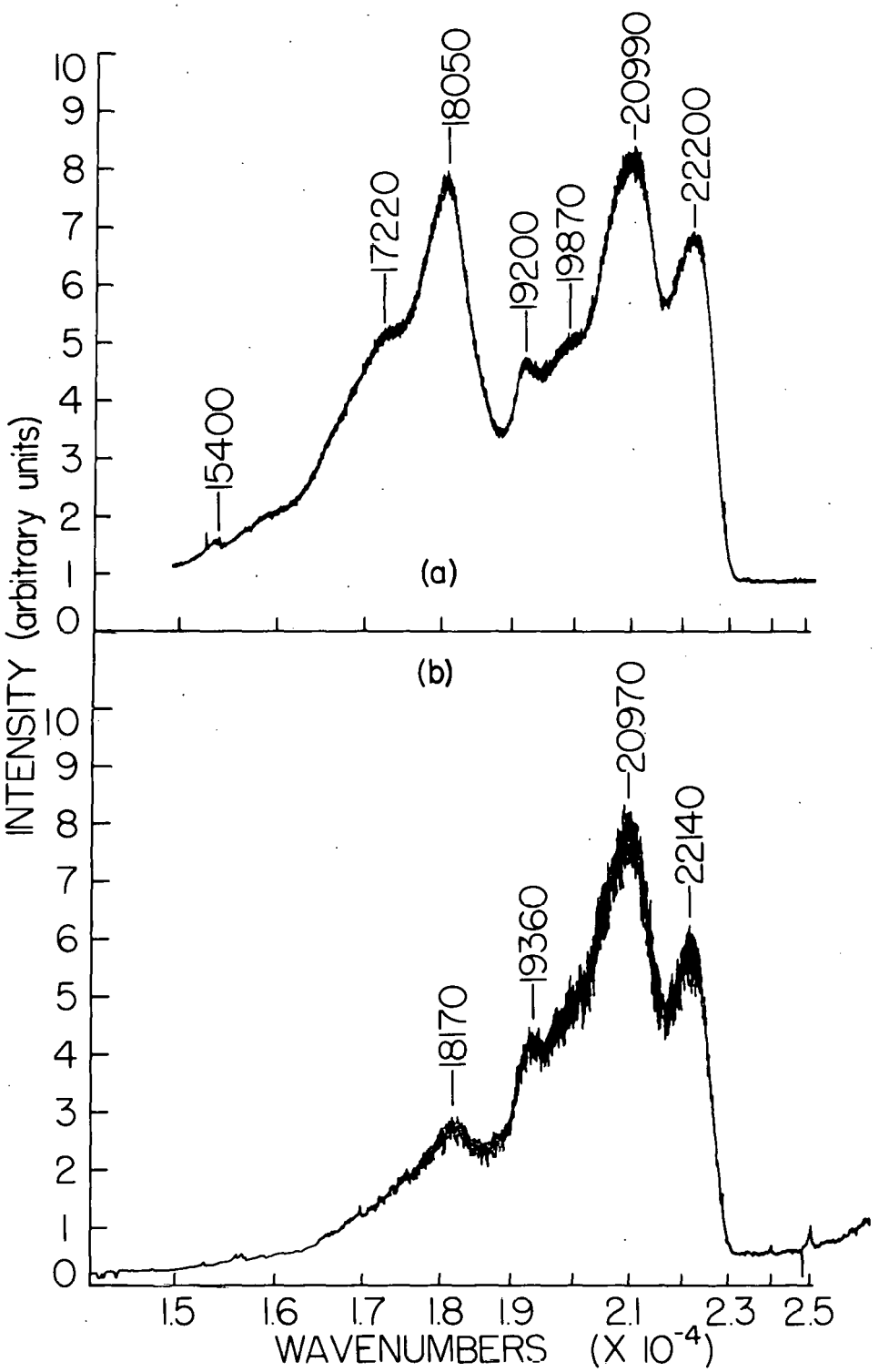

Figure 6. CT emission of (a) .05% and (b) .015% A-PMDA in N-PMDA obtained with 3640 Å (UV) excitation. Peak locations are given in units of cm^{-1}.

Table 1. UV and visible excitation of A-PMDA and Py-PMDA guests and the N-PMDA host

Crystal	Peak Locations (cm^{-1})	
	UV Excitation	Visible Excitation
.05% A-PMDA	22,200	
	20,990	
	19,870	
	19,200	
	18,040	18,090
	17,210	17,160
		15,401
		15,010
.015% A-PMDA	22,160	
	20,940	
	19,340	
	18,170	17,990
		17,160
		15,401
		15,010
Neat N-PMDA	22,180	
	20,980	
	19,360	
.015% Py-PMDA	22,160	
	20,900	
	19,830	
	17,870	See Table 2

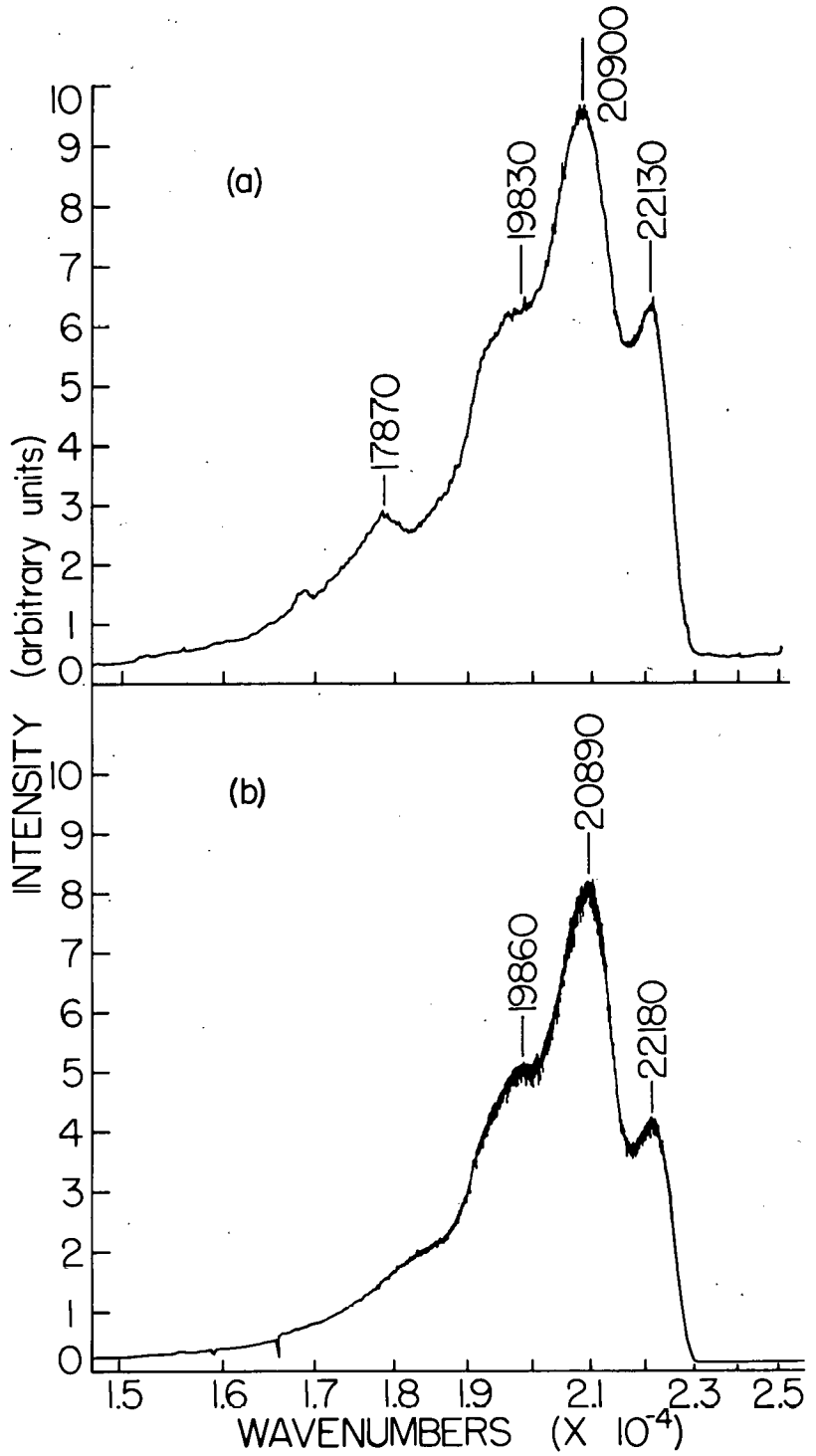

Figure 7. CT emission of (a) .015% Py-PMDA in N-PMDA and (b) neat N-PMDA obtained with 3640 Å (UV) excitation. Peak locations are given in units of cm^{-1}.

The .015% A-PMDA crystal gives a poorly resolved peak at 18,170 cm^{-1} while the .05% crystal shows a peak at 18,050 cm^{-1} and a shoulder at $\sim$17,220 cm^{-1}. These are attributed to A-PMDA fluorescence. The dependence of peak locations on impurity concentration will be discussed later. However, the visible excitation spectra of A-PMDA given in Figure 8 shows that the values of $\sim$18,050 cm^{-1} and $\sim$17,160 cm^{-1} given there match the .05% spectrum more closely.

Visible excitation of A-PMDA guest

The visible excitation spectra shown in Figure 8 demonstrate that for a given crystal there is no dependence of the emission on the exciting frequency between 4579 Å and 5145 Å. The energy separation between the two most intense bands (located at $\sim$18,000 cm^{-1} and 17,160 cm^{-1}) varies from 835 cm^{-1} for the .05% crystal to 925 cm^{-1} for the .015% sample. This range of values is significantly less than the spacing of 1310 cm^{-1} reported for neat crystals of A-PMDA (56).

Differences in crystal spectra

The differences in band positions and associated energy spacings of the two concentrations of A-PMDA in N-PMDA mentioned above is unusual for mixed organic crystal systems. The degree to which these differences can be attributed to concentration effects is uncertain. The 3640 Å excitation

spectra, especially the .015% A-PMDA spectrum shown in Figure 6b, show much more "noise" than spectra of the same crystals using visible excitation but noise alone cannot account for the differences. It should be noted that the angle of incidence of the laser onto each sample was varied in order to maximize the signal-to-noise ratio and minimize scattered laser light. The excess noise in the 3640 Å spectra is, in part, attributed to an inconsistent instability in the 3640 Å laser line.

Even in relatively "noise-free" fluorescence spectra, such as those of Figure 8 obtained with visible excitation, there are significant differences in peak positions. A good example is the $\sim$18,000 cm^{-1} peak attributed to A-PMDA fluorescence. Different crystals of $\sim$.05% A-PMDA concentration show the peak maximum anywhere from 17,990 cm^{-1} to 18,100 cm^{-1}, a range of $\sim$110 cm^{-1}. The location of the maximum of each particular crystal is reproducible, however, and does not shift as the excitation wavelength is varied from 4579 Å to 5145 Å. The halfwidth of this peak also varies from crystal to crystal, but a trend of a greater halfwidth ($\sim$150 cm^{-1}) for peaks in the 18,100 cm^{-1} region (<u>versus</u> a halfwidth of $\sim$120 cm^{-1} for peaks with a 17,990 cm^{-1} maximum) seems to follow. The spectra shown in Figure 8, therefore, are respresentative of the differences obtained in peak locations although the differences cannot be attributed solely to concentration effects.

Figure 8. CT emission of (a) 4579 Å excitation of .05%, (b) 5145 Å excitation of .05%, (c) 4579 Å excitation of .015%, and (d) 5145 Å excitation of .015% A-PMDA in N-PMDA. Peak locations are given in units of cm^{-1}.

THIS PAGE

WAS INTENTIONALLY

LEFT BLANK

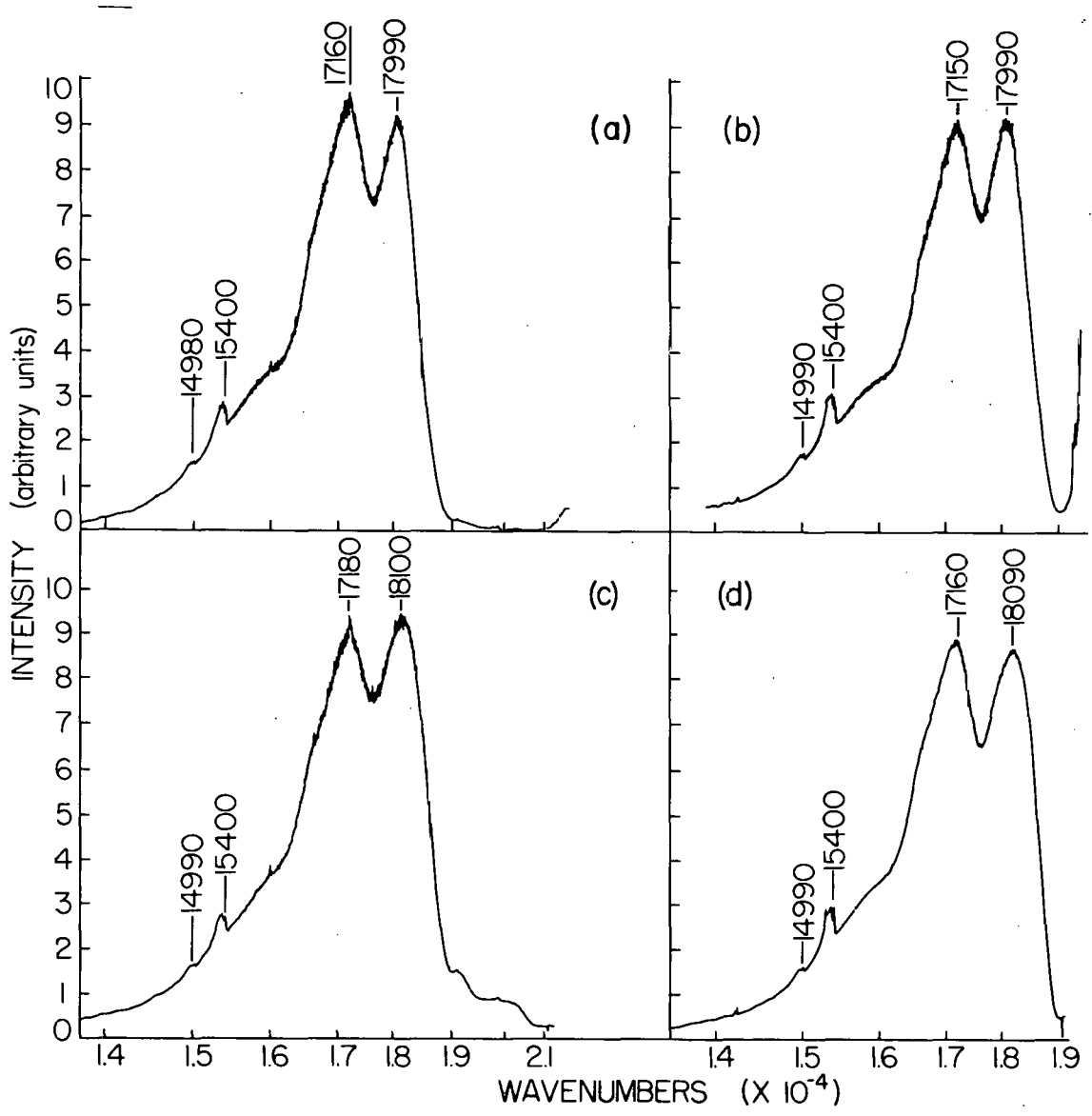
(a)
(b)
(c)
(d)
17160
17990
14980
15400
17150
14990
17180
18100
18090
INTENSITY (arbitrary units)
WAVENUMBERS (X 10⁻⁴)
0
1
2
3
4
5
6
7
8
9
10
1.4
1.5
1.6
1.7
1.8
1.9
2.1

The differences in peak locations and bandwidths are probably due to the disordering of the N-PMDA and differences in crystal quality. Increasing the guest concentration in N-PMDA may increase the amount of disordering. It is possible that the A-PMDA molecules preferentially occupy certain sites until, at higher concentrations, all such sites are filled and the remaining molecules are forced into less desirable orientations. However, there is no conclusive evidence of this and a much more detailed study is required before such an assertion can be made.

Finally, it should be noted that there is no sharp vibronic structure observed in the fluorescence spectrum of A-PMDA in N-PMDA, which is consistent with the lack of sharp structure in the absorption spectrum. We will next discuss the observed phosphorescence spectrum which provides more interesting information.

Phosphorescence of A-PMDA

The visible excitation spectra of A-PMDA show a weak emission at 15,400 cm^{-1} and (15,400-391) cm^{-1}, which is attributed to anthracene phosphorescence. An expanded spectrum of this region is shown in Figure 9. The zero-phonon band of the phosphorescence origin, located at 15,401 cm^{-1}, is accompanied by a three member phonon progression. The zero-phonon transition of the first vibrational band at 391 cm^{-1} is visible and located at

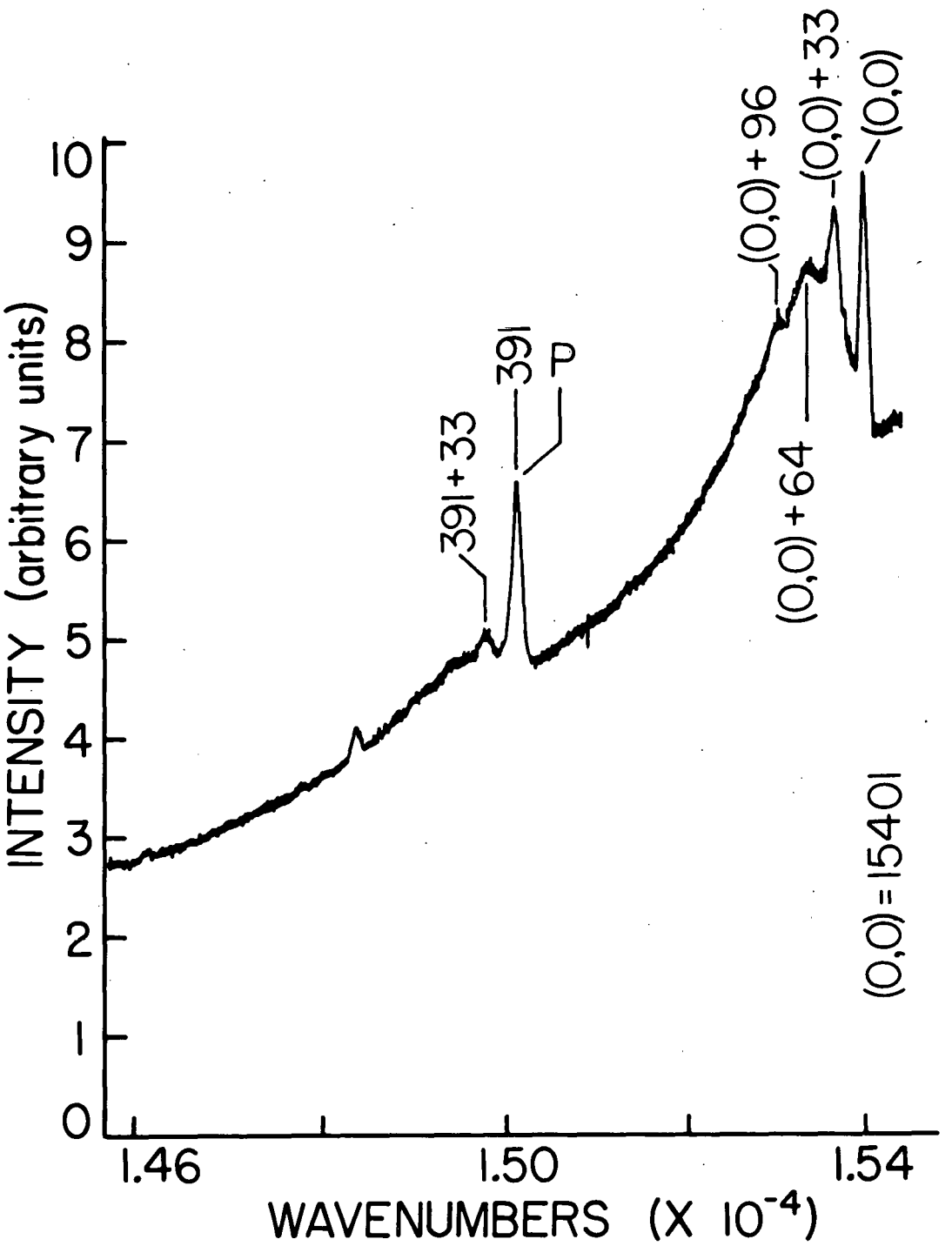

Figure 9. Phosphorescence of .015% A-PMDA in N-PMDA obtained from 4880 Å excitation. Peak locations are given in units of cm^{-1}, T ≈ 2°K.

15010 cm^{-1} although it unfortunately suffers interference from a laser plasma line. The vibrational spacing of 391 cm^{-1} is approximately equal to the 396 cm^{-1} spacing reported by Haarer, et al. (68) in their study of neat A-PMDA crystals and to the 396 cm^{-1} value reported for the anthracene phosphorescence in a phenazine host (69).

The bandwidths for the zero-phonon and one-phonon transitions of the origin region could not be accurately measured due to slit broadening. An effective slit width of 1.2 Å was required to measure the weak signal.

Blue shift of phosphorescence

The phosphorescence origin at 15,401 cm^{-1} is blue shifted by $\sim$715 cm^{-1} from the 14,686 cm^{-1} origin (69) observed for anthracene in a phenazine host. The energy in the phenazine host should be a good approximation to the "free molecule" phosphorescent state energy. Haarer, et al. (68) report a phosphorescence origin at 15,493 cm^{-1} which is blue shifted an additional 90 cm^{-1} from our mixed crystal study. A brief synopsis of the explanation given by these authors for the unexpected blue-shift will be given below.

The key to the explanation given by Haarer, et al. (68) is the small overlap between the "free molecule" anthracene triplet state and the lowest lying triplet CT state of the complex. To understand why the overlap is small, we must consider the orbitals involved and their symmetry. In the

free complex, the long axes of both the anthracene and PMDA molecules are parallel to each other and the plane containing these two long axes is perpendicular to their molecular planes. Now, the triplet state of a "free molecule" of anthracene results from the transfer of an electron from the highest occupied orbital (HOMO) of anthracene to the lowest unoccupied orbital (LUMO) of anthracene. This triplet state is denoted as $E(^3L)$.

It is assumed that the lowest lying excited CT state is formed from the promotion of an electron from the HOMO of anthracene to the LUMO of PMDA.

If one considers the symmetry of the final states of the transitions for the "free molecular" anthracene and the CT triplet states, one finds that the LUMO of anthracene (in the anthracene triplet) and the LUMO of PMDA (in the CT triplet) are of opposite symmetry with respect to reflection in the symmetry plane containing the long axes of both molecules. Therefore, the overlap between the triplet states of anthracene and the CT complex is very small. If the symmetry plane containing the long axes was perpendicular to the molecular plane, the overlap would be exactly zero. This arrangement, however, is not perfectly maintained in the crystalline environment.

The HOMO of anthracene and the LUMO of PMDA, which are the orbitals involved in the formation of the lowest CT

excited state are of the same symmetry with respect to reflection and this results in a nonzero overlap between the ground state and the lowest singlet state of the CT complex.

The consequence of the above reasoning is that the matrix element of the hamiltonian between the two singlet states (ground and first excited), V_1, is much larger than the matrix element, V_3, governing the interaction between the two triplet states. This difference is the dominant factor in the expressions (68)

$$\Delta_T = \frac{V_3^2}{E(^3A^-D^+) - E(^3L)} \simeq \frac{V_3^2}{2500\ cm^{-1}} \tag{35}$$

and

$$\Delta_S = \frac{V_1^2}{E(^1A^-D^+) - E(AD)} = \frac{V_1^2}{18{,}000\ cm^{-1}} \tag{36}$$

where $2\Delta_S$ gives the shift caused by mixing the unperturbed ground state E_{AD} of the CT state with its unperturbed "ionic" state $E(^1A^-D^+)$ and $2\Delta_T$ gives the shift caused by mixing the ionic CT triplet $E(^3A^-D^+)$ with the unperturbed localized triplet $E(^3L)$.

If the matrix elements V_1 and V_3 were of equal magnitude, the larger denominator of Δ_S would result in a red shift. However, since $V_3 << V_1$, the difference in the denominators is no longer large enough to compensate for the difference in the numerators and a blue shift occurs.

Emission of Py-PMDA in N-PMDA

The emission spectra of .015% Py-PMDA in N-PMDA are given in Figures 7a and 10-12.

UV excitation of Py-PMDA guest in N-PMDA host

The 3640 Å excitation spectrum of .015% Py-PMDA in N-PMDA given in Figure 7a shows peaks at 22,130 cm^{-1}, 20,900 cm^{-1} and 19,830 cm^{-1} which are attributed to the N-PMDA host CT fluorescence. There is a weak emission at 17,870 cm^{-1}. This peak is not present in any of the visible excitation (4579 Å - 5145 Å) spectra. It would seem reasonable to attribute this peak to fluorescence of Py-PMDA. If this were so, one would expect to see the same or a smaller intensity ratio of fluorescence to phosphorescence with visible excitation as with 3640 Å excitations since the mechanism for intersystem crossing from the singlet CT state to the triplet CT state is presumably the same regardless of the way the CT singlet state is populated. In addition, if one assumes that the 17,870 cm^{-1} peak is Py-PMDA CT fluorescence, the Stokes shift between this peak and the lowest absorption peak at 18,330 cm^{-1} would only be $\sim$460 cm^{-1}. This value indicates a much smaller Stokes shift than is expected for this complex. For these reasons, then, the 17,870 cm^{-1} peak remains unexplained.

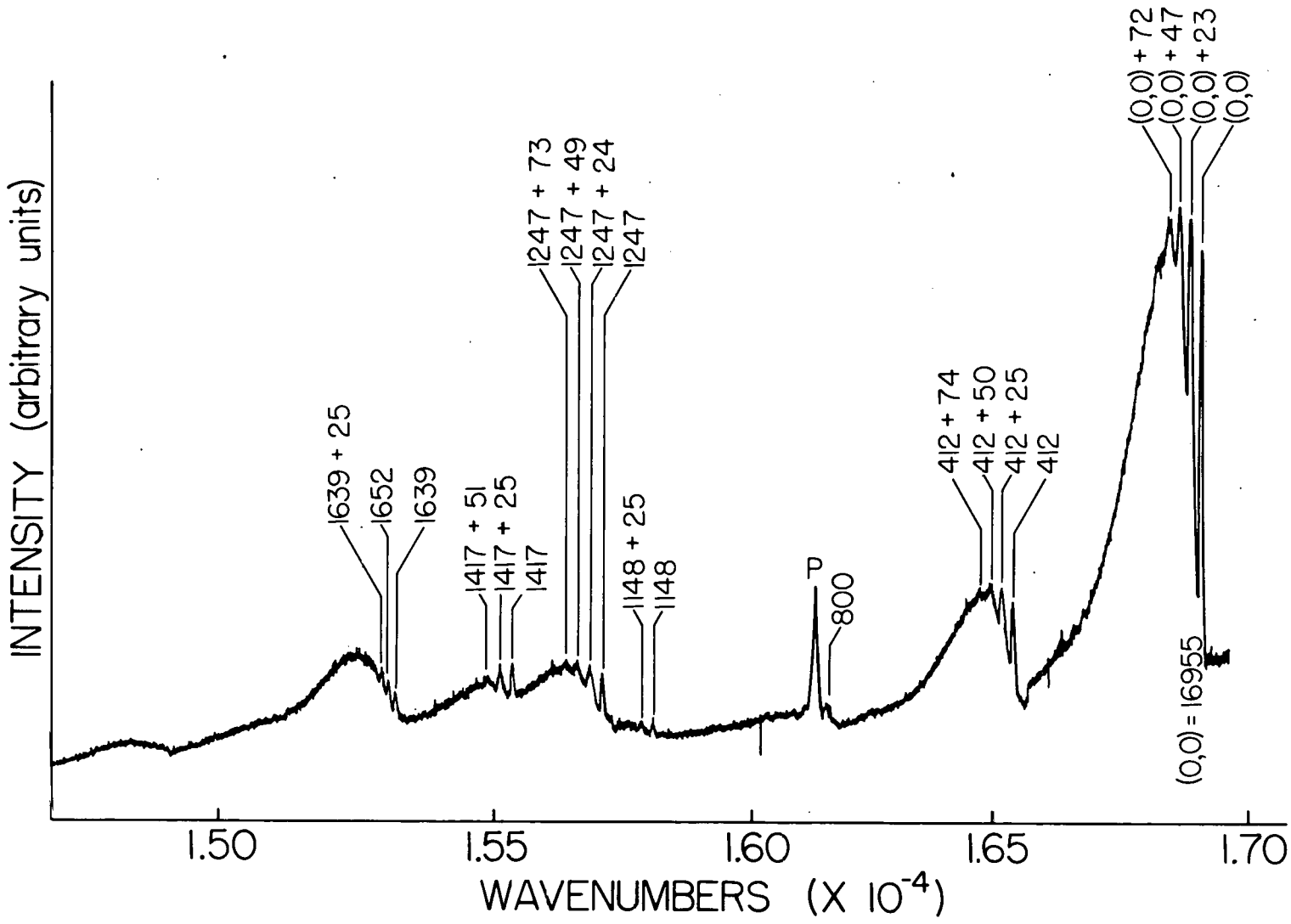

Figure 10. Phosphorescence spectrum of .015% A-PMDA in N-PMDA obtained from 4880 Å excitation. Peak locations are given in units of cm^{-1}.

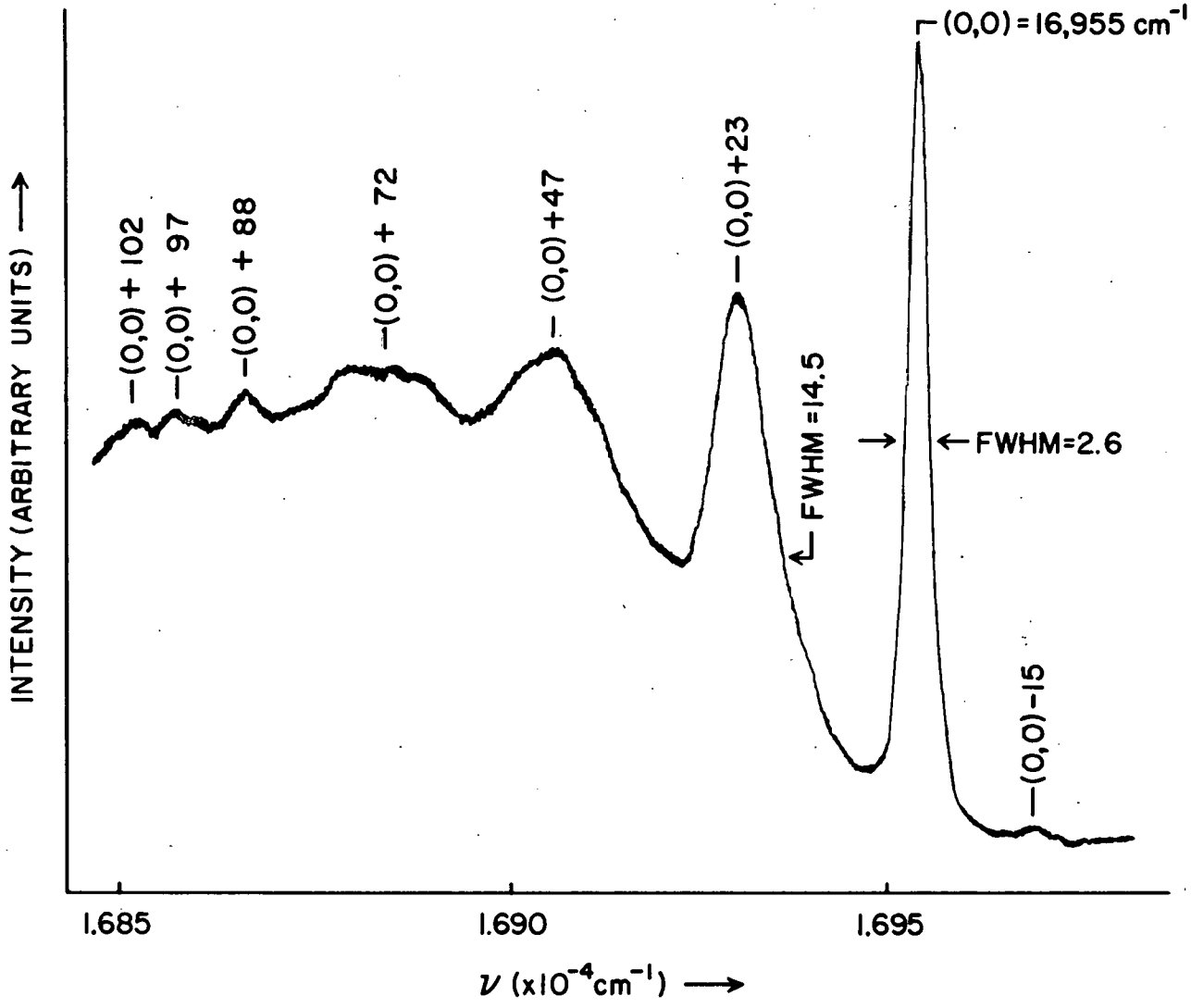

Figure 11. Phosphorescence of Py-PMDA in N-PMDA showing the region near the origin band. Note the hot band (ω_T = 15 cm^{-1}) to the high energy side of the (0,0) band. Exciting wavelength = 4880 Å, T ∿2°K.

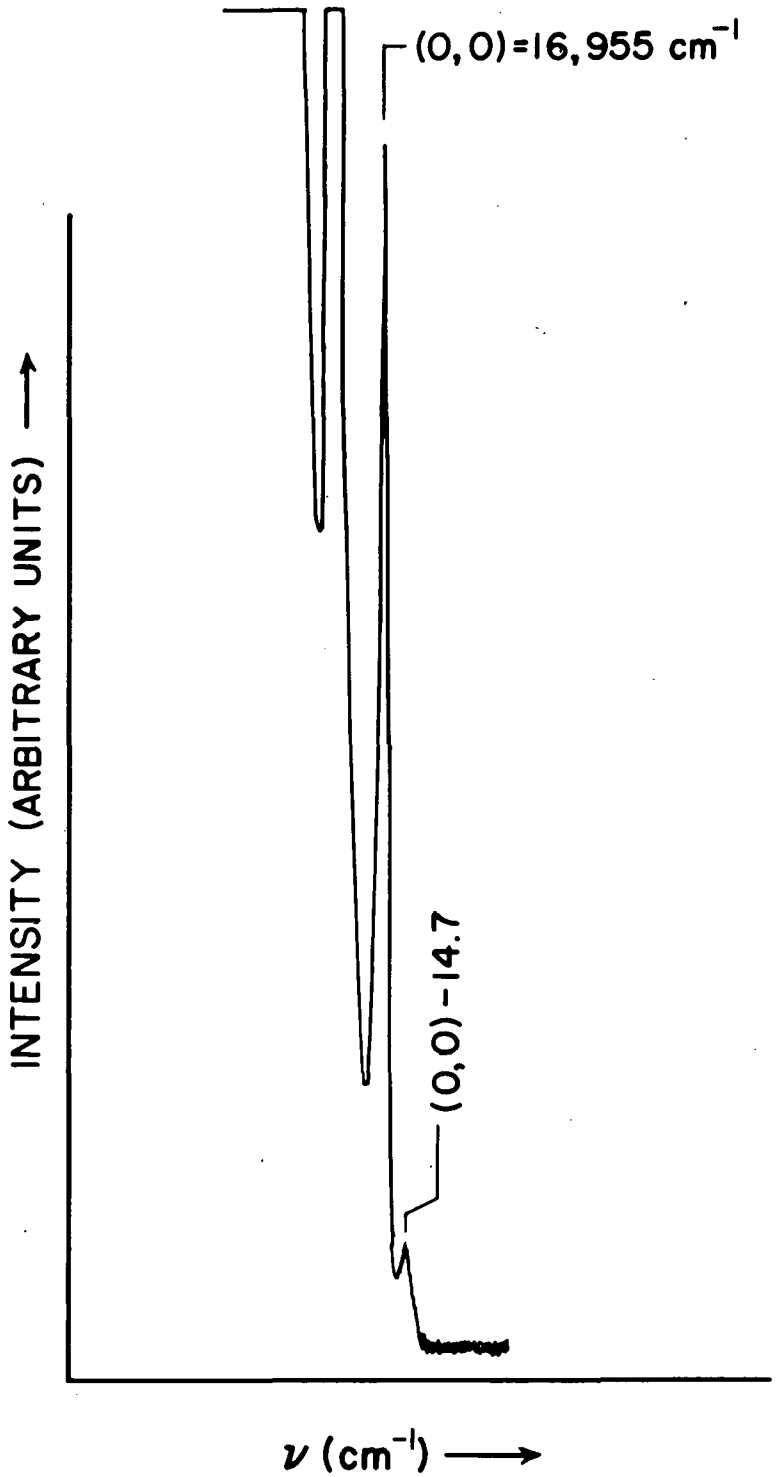

Figure 12. Phosphorescence of Py-PMDA in N-PMDA showing a "hot band" phonon transitions (ω_T = 14.7 cm^{-1}) to the high energy side of the zero-phonon origin band (0,0). Excitation wavelength = 4880 Å, T ∿6°K.

Phosphorescence of Py-PMDA

The phosphorescence spectrum of Py-PMDA in N-PMDA, which is shown in Figure 10, is independent of excitation wavelength in the range 4579 Å to 5145 Å. The origin band is located at 16,955 cm^{-1} (uncorrected to vacuum). The frequencies listed in Table 2 correspond to ground state fundamental vibrations. The phosphorescence of pyrene has been studied in the vapor phase (70), in a rigid matrix (71) (ethanol at 77°K) and in a neat crystal (72,73). None of these studies give sharp vibrational structure and with the reported full-width-half-maxima (FWHM) of ca. 100 cm^{-1}, one can only expect an agreement between our data and the published frequencies of several wavenumbers. Thus, the agreement given in Table 2 indicates that the phosphorescence of the Py-PMDA can be qualitatively associated with the pyrene donor (but see below for further discussion).

Shift of the phosphorescence origin

We observe a phosphorescence origin band at 16,955 cm^{-1}. Within the uncertainties resulting from the broad spectra reported in the literature (70-73), we report that there is no appreciable shift between our origin location and the literature values. This may seem surprising since the A-PMDA complex exhibited such a large blue shift. However, recall that the focus of the explanation presented earlier is on the small overlap between the triplet CT state and the

Table 2. Comparison of Py-PMDA and pyrene vibrational progressions

Py-PMDA Vibrational Origin (cm^{-1})	Pyrene Vibrational Origin (cm^{-1})
412	410
800	790
1148	---
1247	1250
1417	---
1639	1620
1652	---

unperturbed localized (anthracene) triplet state. For A-TCNB (tetracyanobenzene), EPR data predicts only 5% (52) CT character in the lowest triplet state of the complex. For Py-TCNB, a 36% (50) CT contribution is measured. We will assume the same relative ratios exist in the PMDA system, that is, the pyrene donor makes a larger contribution to the observed triplet state than does anthracene. Part of this increase can be attributed to a greater overlap between the charge transfer triplet and the localized (pyrene) triplet. Thus, one would not expect the matrix element V_3 given in eq. (35) to be much smaller than V_1 and, consequently, one would not expect a blue shift to occur.

Ground state and excited state phonon energies

With the exception of the 800 cm^{-1} band, each of the remaining vibrational peaks display a striking phonon progression in a 25 cm^{-1} mode. Three members of the phonon progression are evident in Figure 10. The spectra shown in Figures 11 and 12 correspond to a sample temperature of ~2°K and ~6°K, respectively, and reveal a weak band lying 14.7 cm^{-1} to higher energy of the origin at 16,955 cm^{-1}. The band is significantly diminished in intensity in going from 6°K to 2°K, indicating that it is a hot band. This hot band undoubtedly originates from the one-quantum level of the phonon in the phosphorescent state (frequency of 14.7 cm^{-1}) and terminates at the zero-phonon level of the ground electronic state, vide infra. In other words, we suggest that a phonon frequency which is 24.6 cm^{-1} in the ground electronic state suffers an unusually large decrease to 14.7 cm^{-1} in the excited state. To our knowledge, such an observation is unprecedented.

Calculation of the electron-phonon coupling strength S

Using equation (34) given in the theory section and the measured areas of the zero-phonon and first-phonon transitions (of Figure 11 at 2°K), the electron-phonon coupling strength is calculated to be $S \simeq 2.5$. This indicates intermediate strength electron-phonon coupling in the triplet state.

However, this calculation is based upon the assumption that the force constant k, which is related to the observed phonon energy by

$$\omega = \sqrt{k/m_{PMDA}} \tag{37}$$

(m_{PMDA} being the weight of a PMDA molecule), is the same for the ground and first excited states. From the frequencies $\omega_T = 14.7\ cm^{-1}$ and $\omega_G = 24.6\ cm^{-1}$ reported above, this obviously is not so. We, therefore, derive a more appropriate expression for the electron-phonon coupling parameter S.

For the ground state, the potential energy is taken to be that of a simple harmonic oscillator, i.e.,

$$E_G(Q) = E_G(0) + \tfrac{1}{2}\, bQ^2 \tag{38}$$

where Q is the "mass weighted" normal coordinate associated with the $24.6\ cm^{-1}$ mode. The excited state potential energy E_T can be expressed in terms of Q as

$$\begin{aligned} E_T(Q) &= E_T(0) + AQ + \tfrac{1}{2}\, BQ^2 \\ &= (E_T(0) - \tfrac{1}{2}\,\tfrac{A^2}{B}) + \tfrac{1}{2}\, B(Q + \tfrac{A}{B})^2 \end{aligned} \tag{39}$$

where ω_T is the circular frequency ($= B^{1/2}$) and

$$Q_T = Q + \frac{A}{B} \tag{40}$$

is the new normal coordinate for the excited triplet state. Referring to Figure 13 and equation (40), we see that

$$\Delta Q = Q_T - Q = \frac{A}{B} \tag{41}$$

is the shift of the potential well minimum between the ground and excited states. The quantity ΔQ can be evaluated by using standard Frank-Condon factor computations as outlined by C. Manneback (74). For $\delta = (\frac{\omega_G}{\omega_T})^{1/2} = 1.3$ and a relative intensity ratio of the one-phonon to zero-phonon bands of 2.5 (for T = 2°K), the calculation yields

$$\Delta Q = 4.526 \times 10^{-20} \text{ gm}^{1/2} \text{ cm} \tag{42}$$

We now define the electron-phonon coupling parameter S as (75)

$$S = \frac{1}{2} (\frac{\omega}{\hbar})(\Delta Q)^2 \tag{43}$$

When the ground and excited state phonon energies are equal, there is no ambiguity about the choice of ω. For our case, we will calculate two values of S, S' for the excited state frequency ω_T and S" for the ground state frequency ω_G. They are

$$S' = 2.6 \quad \text{and} \quad S'' = 4.5$$

These values predict stronger coupling than is predicted by Pryce's model (65).

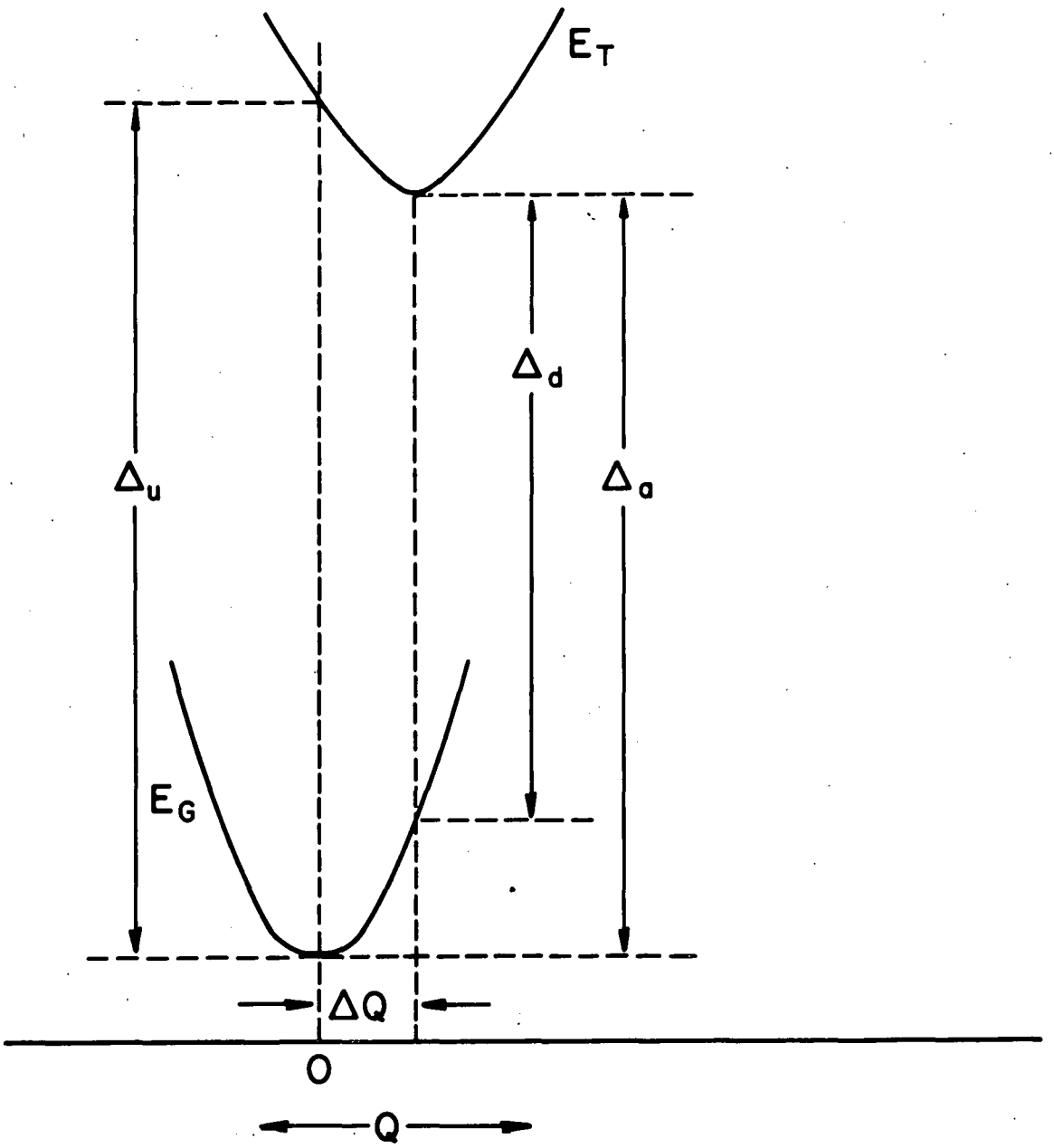

Figure 13. Schematic representation of the ground and excited state potential energy curves showing the energy differences referred to in the model calculations (see text).

Calculation of Stokes shift for the observed phonon mode

The Stokes shift due to the change in the force constant and the shift of the equilibrium separation of the donor-acceptor molecules for the particular mode observed in the phosphorescence can also be calculated. Note from equation (39) and Figure 13 that

$$\Delta_u - \Delta_a = \frac{1}{2}\frac{A^2}{B} = \frac{1}{2} B(\Delta Q)^2 \tag{44}$$

From the definition of B and equation (43), we find

$$\Delta_u - \Delta_a = \hbar S' \omega_T = 39.5 \text{ cm}^{-1} \tag{45}$$

Also note that

$$\Delta_a - \Delta_d = \frac{1}{2} b(\Delta Q)^2 \tag{46}$$

where $\sqrt{b} = \omega_G$. Again, using equation (43) we find

$$\Delta_a - \Delta_d = \hbar S'' \omega_G = 111 \text{ cm}^{-1} \tag{47}$$

The sum of equations (45) and (47) give a total Stokes shift of $\sim$150 cm^{-1}. We emphasize that this is the Stokes shift for the single mode corresponding to the striking phonon progression in Figure 10.

Calculation of bond contraction and assignment of the observed DA mode at $\omega_G = 25 \text{ cm}^{-1}$

Notice that we have not yet specified the motion of the Py-PMDA complex responsible for the principle phonon

progression observed in the phosphorescence spectrum. We start by assuming that the motion responsible for the observed phonon mode is a symmetric stretch between the donor and the neighboring acceptors shown in Figure 14.

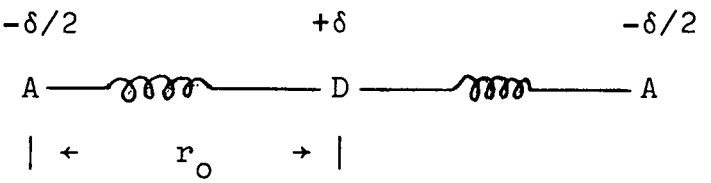

Figure 14. Symmetric stretch of a donor with its neighboring acceptors, with the indicated fractional charge transferred (δ) and the ground state interplanar separation r_o.

We will use two different models to calculate the shift of the equilibrium position upon excitation and then see if the observed frequency reduction for the excited state phonon is predicted by this shift.

We define the change in the interplanar separation of the right acceptor molecule from its ground state equilibrium value as

$$\Delta r_r = r - r_o \tag{48}$$

where r_o is the equilibrium ground state interplanar separation between the donor and acceptor. A crystallographic study of pure Py-PMDA reports r_o = 3.3 Å (76). The change in

interplanar separation for the acceptor to the donor's left, Δr_ℓ, will be equal to Δr_r. We further assume that the motions of the two acceptors are not coupled to each other.

Using the model discussed earlier, we have the normal "mass-weighted" coordinate Q given as

$$Q = \left(\frac{m_{PMDA}}{2}\right)^{\frac{1}{2}} [\Delta r_\ell + \Delta r_r] \tag{49}$$

The change in Q is given as

$$\Delta Q = \left(\frac{m_{PMDA}}{2}\right)^{\frac{1}{2}} \triangle [\Delta r_\ell + \Delta r_r]$$

$$\equiv (2\ m_{PMDA})^{\frac{1}{2}}\ \Delta r \tag{50}$$

Using the value for ΔQ given in equation (42), we calculate

$$\Delta r = .16\ \text{Å},$$

that is, each D....A bond contracts .16 Å in the phosphorescent triplet state.

A coulombic model proposed by Haarer (67) can also be used to calculate the donor-acceptor bond contraction upon excitation. In the ground state of the triatomic shown in Figure 14, only a Hookian force exists between the donor and acceptor. The potential energy is given as

$$V_{HO} = \frac{1}{2}\ k\ (R-R_o)^2 \tag{51}$$

where ΔR is related to the normal coordinate displacement Δr (which was defined earlier in equation (50)) by the relation

$$\Delta R = R - R_o = \frac{1}{\sqrt{2}} (\Delta r_\ell + \Delta r_r) = \sqrt{2}\, \Delta r \qquad (52)$$

In the excited state, the transfer of charge from the donor to the acceptor occurs and an attractive coulombic term is introduced as

$$V_c = \frac{-\delta^2}{(r_o + \frac{\Delta R}{\sqrt{2}})} \qquad (53)$$

where δ is defined as the fractional contribution of the CT triplet to the observed phosphorescence triplet. From EPR measurements, this fraction is .36 (50) for Py-TCNB. We will assume the same fractional contribution exists in Py-PMDA as in Py-TCNB. This assumption is justified by the similarity between the two complexes and the simplicity of the coulombic model.

The bond contraction of the donor-acceptor pair can be calculated from the total potential energy $V = V_{HO} + V_c$ by evaluating Δr for $\frac{\partial V}{\partial \Delta R} = 0$. The result is

$$\Delta r_{min} = \frac{\Delta R_{min}}{\sqrt{2}} = -0.20 \text{ Å}$$

Thus, the agreement for the bond contractions given by the two different models is very good.

One can calculate the force constant of the excited state k_{CT} as

$$k_{CT} = \frac{\partial^2 V}{\partial \Delta R^2}\Bigg|_{\Delta R_{min} = -\sqrt{2}\ (.20\ \text{Å})} = 6.77 \times 10^{-2}\ \frac{\text{mdynes}}{\text{Å}}$$

Using equation (37), one predicts a hot band frequency of

$$\omega_T(\text{calc.}) = 23\ \text{cm}^{-1}$$

This value of ω_T(calc.), which predicts only a 1.7 cm^{-1} reduction in the frequency of the hot band, does not give good agreement with the observed value of $\omega_T = 14.7\ \text{cm}^{-1}$ ($\omega_G = 24.6\ \text{cm}^{-1}$). It is true that the coulombic model is oversimplified and longer-range interactions need to be considered. However, we feel that these would only serve to increase the force constant, resulting in an even smaller change of the interplanar D-A separation between the ground and excited states. Therefore, we feel that these calculations show that our original assumption (the symmetric stretch between the donor and its neighboring acceptors is responsible for the observed phonon mode) is not valid, and that some other motion is responsible for the observed results. Haarer (67) has associated a 62 cm^{-1} phonon mode with the symmetric stretch of neighboring PMDA acceptors and the anthracene donor. Since there is a great deal of similarity between A-PMDA and Py-PMDA, we feel the

difference between our 24.6 cm^{-1} phonon energy and his 62 cm^{-1} phonon energy gives further evidence that some other type of motion is responsible for our phonon progression. Also, the phonon mode observed in the weak A-PMDA phosphorescence spectrum is only 32 cm^{-1}, which obviously cannot be due to the same type of donor-acceptor stretch Haarer reports. Figure 11 shows that in the 16,800 cm^{-1} to 16,900 cm^{-1} region there are shoulders and overtone bands which do not fit the $\sim$25 cm^{-1} progression. Whether a second phonon mode associated with a symmetric A-D-A stretch could be present in this region has not been determined.

We suggest, therefore, a rotation of the rigid complex may be the motion associated with the low energy phonon progression observed. Upon excitation, the complex contracts and then has a larger cavity in which to rotate. This would at least qualitatively explain the decrease of the observed excited state phonon frequency relative to the ground state.

Phosphorescence bandwidths

The full-width-half-maxima (FWHM) of the zero-phonon and one-phonon transitions in the phosphorescence origin band shown in Figure 11 are 2.6 cm^{-1} (0.9 Å) and 14.5 cm^{-1} (5.0 Å), respectively. The width of this latter line is obtained by doubling the measured half-width-half-maximum of the high energy side of the band.

The narrow halfwidth of the zero-phonon transition indicates that there is no broadening of the bands due to any disordering that may exist in the N-PMDA. In the N-PMDA, the PMDA molecules may form an ordered lattice while the naphthalene assumes a more random orientation and is responsible for disordering effects. In the mixed crystal, the pyrene impurity's orientation would be dictated by the neighboring PMDA molecules, leaving it unaffected by any disordering of the naphthalene orientation. Such an explanation would account for the observed sharpness of the Py-PMDA phosphorescence.

The 2.6 cm^{-1} FWHM of the zero-phonon transition at 2°K is most likely a measure of the site inhomogeneity and strain broadening of Py-PMDA in N-PMDA. One is entirely justified in asserting that the sources of inhomogeneous line broadening also contribute to the 14.5 cm^{-1} width of the one-phonon band and, furthermore, to the same extent. Therefore, we conclude that the homogeneous linewidth of the one phonon band is ca. 12 cm^{-1}. It has been determined that the high energy side of the one-phonon band profile is Lorenztian to the point where interference of the zero-phonon band onsets. A homogeneous linewidth of 12 cm^{-1} corresponds to a total relaxation time of 0.4 picoseconds for the 25 cm^{-1} one-phonon level of the ground electronic state (where T = relaxation time = $\frac{\Delta E}{\hbar}$).

CONCLUSIONS

The phonon progression observed in the phosphorescence spectrum of Py-PMDA in N-PMDA is, to our knowledge, the first such progression ever reported for a π-molecular CT complex. The electron-phonon coupling strength parameter has been calculated for the ground state (S" = 2.6) and for the excited state (S' = 4.5). Considering that the Py-PMDA CT triplet state makes only a fractional contribution to the observed phosphorescent state, these values indicate strong electron-phonon coupling for the Py-PMDA guest.

A brief phonon progression is observed in the weak phosphorescence spectrum of A-PMDA in N-PMDA also.

For the two mixed crystal systems studied, A-PMDA and Py-PMDA in N-PMDA, we note that the smaller the contribution of the guest's CT triplet state to the observed phosphorescence state, the more the origin of the phosphorescence of the guest complex is blue shifted from the origin of the phosphorescence of the pure donor. The phonon mode frequencies observed in the phosphorescence spectra of mixed crystals of A-PMDA (ω_G = 32 cm^{-1}) and Py-PMDA (ω_G = 24.6 cm^{-1}) in N-PMDA are of much lower energy than the frequency of the mode that Haarer (67) attributes to a symmetric donor-acceptor stretch in neat crystals of A-PMDA. This indicates, as do the results of our model calculations done on Py-PMDA, that the motion responsible for the phonon

progressions we observe are rotations of the rigid guest complexes in the N-PMDA and not symmetric stretches of the donor and acceptor molecules. We interpret the reduction of the phonon mode frequency that occurs upon excitation (as observed in the Py-PMDA mixed crystal only; ω_G = 24.6 cm^{-1} and ω_T = 14.7 cm^{-1}) in terms of a contracted complex that can more easily rotate in what would be a larger cavity.

The CT absorption spectra of A-PMDA and Py-PMDA in N-PMDA are broad and structureless, indicating strong electron-phonon coupling in the guest. The same conclusion is indicated by the structureless CT fluorescence of A-PMDA. We do not observe any CT fluorescence that can be conclusively attributed to Py-PMDA. Apparently, the inter-system crossing mechanism is extremely fast although we have no explanation as to why this is so.

The broad structureless absorption and emission spectra of the lowest N-PMDA excited charge transfer (CT) singlet state indicate strong exciton-phonon coupling in the neat crystal. The particularly long absorption tail observed supports the contention that N-PMDA is disordered. Further study is needed to verify the existence of the disordering and its relationship (if any) to the anomalous absorption bands (23,330 cm^{-1}, 23,060 cm^{-1} and 22,770 cm^{-1}) observed for N-PMDA crystals.

REFERENCES

1. Z. G. Soos, Ann. Rev. Phys. Chem. 25, 121 (1974).

2. L. B. Coleman, M. J. Cohen, D. J. Sandman, F. G. Yamayishi, A. F. Garito and A. J. Heegar, Solid State Commun. 12, 1125 (1973).

3. Physics Today 29(2), 17 (1976).

4. A. J. Heegar and A. F. Garito in Low Dimensional Cooperative Phenomena, edited by H. J. Keller (Plenum Press, New York, 1975).

5. A. J. Heegar and A. F. Garito, Lect. Notes Phys. 34, 151 (1975).

6. M. J. Rice in Low Dimensional Cooperative Phenomena, edited by H. J. Keller (Plenum Press, New York, 1975).

7. M. J. Rice, S. Strassler and W. R. Schneider, Lect. Notes Phys. 34, 282 (1975).

8. R. E. Peierls, Quantum Theory of Solids (Clarendon Press, Oxford, 1955).

9. H. G. Schuster, Lect. Notes Phys. 34, 1 (1975).

10. A. J. Heegar and A. F. Garito, A.I.P. (Amer. Inst. Phys.) Conf. Proc., 1972, 10(2), 1476 (1973).

11. I. F. Shchegolev, Phys. Status Solidi A 12, 9 (1972).

12. K. Yakushi, I. Ikemoto and H. Kuroda, Acta Cryst. B27, 1710 (1971).

13. K. Yakushi, I. Ikemoto and H. Kuroda, Acta Cryst. B29, 2640 (1973).

14. T. Amano, H. Kuroda and H. Akamatu, Bull. Chem. Soc. Jap. 42, 671 (1969).

15. I. J. Tickle and C. K. Prout, J. Chem. Soc., Perkin II, 724 (1973).

16. K. Prout and I. J. Tickle, J. Chem. Soc., Perkin II, 1212 (1973).

17. I. J. Tickle and C. K. Prout, J. Chem. Soc., Perkin II, 731 (1973).

18. M. I. Foreman, R. Foster and C. A. Fyfe, J. Chem. Soc., B, 528 (1970).

19. O. B.Nagy, S. Dupire, J. B.Nagy, Tetrahedron 31, 2453 (1975).

20. S. K. Chakrabarti and S. Basu, Trans. Faraday Soc. 60, 465 (1964).

21. B. Chakrabarti and S. Basu, J. Chim. Phys. 63, 1044 (1966).

22. B. Chakrabarti and S. Basu, J. Chim. Phys. Physiochem. Biol. 65, 1006 (1968).

23. G. T. Pott and J. Kommandeur, Mol. Phys. 13, 373 (1967).

24. M. H. Fisch and W. M. Hemmerlin, Tetrahedron Lett. 31, 3125 (1972).

25. T. Nogami, K. Yoshihara and S. Nagakura, Bull. Chem. Soc. Jap. 45, 122 (1972).

26. S. Koizumi and Y. Matsunaga, Bull. Chem. Soc. Jap. 45, 423 (1972).

27. M. E. Peover and J. D. Davies, Trans. Faraday Soc. 60, 476 (1964).

28. H. Inoue, S. Hayashi and E. Imoto, Bull. Chem. Soc. Jap. 37, 336 (1964).

29. H. Kuroda, K. Yoshihara and H. Akamato, Bull. Chem. Soc. Jap. 35, 1604 (1962).

30. M. Alexandre and P. Rigny, Mol. Cryst. Liq. Cryst. 17, 19 (1972).

31. D. R. Kearns, P. Gardner and J. Carmody, J. Phys. Chem. 71, 931 (1967).

32. F. P. Chen and P. N. Prasad, Chem. Phys. 16, 175 (1976).

33. F. H. Herbstein and M. Kaftory, Acta Cryst. B31, 60 (1975).

34. F. H. Herbstein in Perspectives in Structural Chemistry, edited by J. D. Dunitz and J. A. Ibers (John Wiley & Sons, London, 1971), Vol. 21 and references therein.

35. D. S. Brown, S. C. Wallwork and A. Wilson, Acta Cryst. 17, 168 (1964).

36. J. Tanaka and K. Yoshihara, Bull. Chem. Soc. Jap. 38, 739 (1965).

37. S. K. Lower, R. M. Hochstrasser and C. Reid, Mol. Phys. 4, 161 (1961).

38. R. M. Hochstrasser, S. K. Lower and C. Reid, J. Mol. Spectrosc. 15, 257 (1965).

39. R. M. Hochstrasser, S. K. Lower and C. Reid, J. Chem. Phys. 41, 1073 (1964).

40. R. Beckman, J. Hayes and G. J. Small, Chem. Phys. 21, 135 (1977).

41. T. Kobayashi and S. Nagakura, Bull. Chem. Soc. Jap. 45, 987 (1972), and references therein.

42. S. Matsumoto, S. Nagakura, S. Iwata and J. Nakaura, Chem. Phys. Lett. 13, 463 (1972).

43. N. Mataga and Y. Murata, J. Amer. Chem. Soc. 91, 3144 (1969).

44. T. Kobayashi, K. Yashihara and S. Nagakura, Bull. Chem. Soc. Jap. 44, 2603 (1971).

45. H. Masuhara and N. Mataga, Chem. Phys. Lett. 22, 305 (1973).

46. H. Möhwald and E. Sackmann, Chem. Phys. Lett. 21, 43 (1973).

47. H. Möhwald and E. Sackmann, Chem. Phys. Lett. 26, 509 (1974).

48. P. Krebs, E. Sackmann and J. Schwarz, Chem. Phys. Lett. 8, 417 (1971).

49. H. Hayashi, S. Iwata and S. Nagakura, J. Chem. Phys. 50, 993 (1969).

50. H. Möhwald and E. Sackmann, Z. Naturforsch., A 29, 1216 (1974).

51. H. Beens, J. de Jong and A. Weller, Colloque Ampere 15, 289 (1969).

52. N. S. Dalal, D. Haarer, J. Bargon and H. Möhwald, Chem. Phys. Lett. 40, 326 (1976).

53. H. Möhwald and A. Böhm, Z. Naturforsch., A 31, 1324 (1976).

54. H. Möhwald and A. Böhm, Chem. Phys. Lett. 43, 49 (1976).

55. D. Haarer and N. Karl, Chem. Phys. Lett. 21, 49 (1973).

56. D. Haarer, Chem. Phys. Lett. 27, 91 (1974).

57. D. Haarer, Chem. Phys. Lett. 31, 192 (1975).

58. D. Haarer, M. R. Philpott and H. Morawitz, J. Chem. Phys. 63, 5238 (1975).

59. P. J. Strebel and Z. G. Soos, J. Chem. Phys. 53, 4077 (1970).

60. R. S. Mulliken, J. Amer. Chem. Soc. 74, 811 (1952).

61. R. S. Mulliken and W. B. Person, Ann. Rev. Phys. Chem. 13, 107 (1962).

62. M. Clarke, D. P. Craig and L. A. Dissado, to be published.

63. A. S. Davydov, Theory of Molecular Excitons (Plenum Press, New York, 1971).

64. D. P. Craig and L. A. Dissado, Chem. Phys. 14, 89 (1976).

65. M. H. L. Pryce in Phonons in Perfect Lattices and in Lattices with Point Imperfections, edited by R. W. H. Stevenson (Oliver and Boyd, London, 1966).

66. D. B. Fitchen, R. H. Silsbee, T. A. Fulton and E. L. Wolf, Phys. Rev. Lett. 11, 275 (1963).

67. D. Haarer, J. Chem. Phys., in press.

68. D. Haarer, C. P. Keijzers and R. Silbey, J. Chem. Phys. 66, 563 (1977).

69. R. H. Clarke, J. Chem. Phys. 52, 2328 (1970).

70. W. H. Van Leeuwen, J. Langelaar and J. D. W. Van Voorst, Chem. Phys. Lett. 13, 622 (1973).

71. J. Langelaar, P. P. H. Rettschnick and G. J. Hoijtink, J. Chem. Phys. 54, 1 (1971).

72. O. L. J. Gijzeman, J. Langelaar and J. D. W. Van Voorst, Chem. Phys. Lett. 5, 269 (1970).

73. L. Peter and G. Vaubel, Chem. Phys. Lett. 21, 158 (1973).

74. C. Manneback, Physica XVII, 1001 (1951).

75. G. J. Small, J. Chem. Phys. 52, 656 (1970), and references therein.

76. F. H. Herbstein and J. A. Snyman, Phil. Trans. Roy. Soc., A 264, 635 (1969).

ACKNOWLEDGEMENT

If I were to thank all the people who have helped me professionally or otherwise, this indeed would be a very lengthy acknowledgement. However, I would like to thank certain friends and associates whose help has been indispensable.

First of all, I must thank my major professor, Dr. G. J. Small, for his guidance and encouragement. Drs. J. M. Hayes and V. Sethuraman have also contributed greatly to my work here and must be thanked.

Also, I would like to thank Gary Wells, Harry Amenson, Jerry Hand and Thomas Johnson of the machine shop, Harold Hall, Edgar Moore, Charles Patterson and Evert McKenna of the glass shop, and Scott Smay for their help. Also, my typist, Sue Musselman, deserves a special thanks and some sort of award for tolerating all the changes.

To Steve Thomas, Tom and Gloria Bachmann, Gerald Dishon, the people of SRC/Michaels and all of my other friends, I also extend my thanks. Finally, there are the people who have made contributions that only I can fully recognize. There are Terry Hardt and my parents, Lee and Jean, to whom this thesis is dedicated for teaching me the importance of this life and the friends in it.